NAVAL POSTGRADUATE SCHOOL

MONTEREY, CALIFORNIA

THESIS

ASSESSMENT OF HYBRID COORDINATE MODEL VELOCITY FIELDS DURING AGULHAS RETURN CURRENT 2012 CRUISE

by

Jonathan A. Savage

June 2013

Thesis Co-Advisors: Mary Batteen
Jeffrey W. Book
Robin Tokmakian

Approved for public release; distribution is unlimited

THIS PAGE INTENTIONALLY LEFT BLANK

REPORT DOCUMENTATION PAGE	Form Approved OMB No. 0704-0188

1. AGENCY USE ONLY *(Leave blank)*	2. REPORT DATE	3. REPORT TYPE AND DATES COVERED
	June 2013	Master's Thesis

4. TITLE AND SUBTITLE
ASSESSMENT OF HYBRID COORDINATE MODEL VELOCITY FIELDS DURING AGULHAS RETURN CURRENT 2012 CRUISE

5. FUNDING NUMBERS

6. AUTHOR(S) Jonathan A. Savage

7. PERFORMING ORGANIZATION NAME(S) AND ADDRESS(ES)
Naval Postgraduate School
Monterey, CA 93943-5000

8. PERFORMING ORGANIZATION REPORT NUMBER

9. SPONSORING /MONITORING AGENCY NAME(S) AND ADDRESS(ES)
N/A

10. SPONSORING/MONITORING AGENCY REPORT NUMBER

11. SUPPLEMENTARY NOTES The views expressed in this thesis are those of the author and do not reflect the official policy or position of the Department of Defense or the U.S. government. IRB Protocol number ___N/A_____.

12a. DISTRIBUTION / AVAILABILITY STATEMENT	12b. DISTRIBUTION CODE
Approved for public release; distribution is unlimited	A

13. ABSTRACT (maximum 200 words)
Performance of the Navy's latest operational ocean forecast model (the Hybrid Coordinate Model, HYCOM, which became operational in March 2013) is systematically evaluated by comparing its velocity fields with actual ADCP velocities collected during a two-week cruise in the Agulhas Return Current region in 2012 (ARC 12). This chaotic region is complex and highly variable, with velocities sometimes exceeding 200 cm/s. Assessment using in-situ velocity measurements is very rare. This analysis characterizes the uncertainty in the model output and its predictions that Undersea Warfare operators, as well as other warfighters, obtain from the HYCOM output, and use in real world operations. Qualitative comparisons show good placement by HYCOM of persistent and energetic ocean current and eddy features, but difficulty (as expected, because HYCOM cannot resolve features finer than eddy scale) resolving the finer-scale variability present in the chaotic ARC region. Quantitative comparisons showed that the overall Root Mean Squared Error (RSME) is 35 cm/s and 47˚ near-surface, and 17 cm/s and 32˚ at 500 m depth, showing a general decrease of RMSE with depth.

14. SUBJECT TERMS	15. NUMBER OF PAGES
Ocean Model, HYbrid Coordinate Ocean Model, HYCOM, Model-data Comparison, Ocean Comparison, Acoustic Doppler Current Profiler, ADCP, ADCP-Model comparison, Agulhas Return Current, Agulhas Return Current 2012 Cruise, ARC12, Operational Model	97
	16. PRICE CODE

17. SECURITY CLASSIFICATION OF REPORT	18. SECURITY CLASSIFICATION OF THIS PAGE	19. SECURITY CLASSIFICATION OF ABSTRACT	20. LIMITATION OF ABSTRACT
Unclassified	Unclassified	Unclassified	UU

NSN 7540-01-280-5500 Standard Form 298 (Rev. 2-89)
Prescribed by ANSI Std. 239-18

THIS PAGE INTENTIONALLY LEFT BLANK

Approved for public release; distribution is unlimited

ASSESSMENT OF HYBRID COORDINATE MODEL VELOCITY FIELDS DURING AGULHAS RETURN CURRENT 2012 CRUISE

Jonathan A. Savage
Lieutenant Commander, United States Navy
B.S., United States Naval Academy, 2002

Submitted in partial fulfillment of the
requirements for the degree of

MASTER OF SCIENCE IN METEOROLOGY AND PHYSICAL OCEANOGRAPHY

from the

NAVAL POSTGRADUATE SCHOOL
June 2013

Author: Jonathan A. Savage

Approved by: Mary Batteen
Thesis Co-Advisor

Jeffrey W. Book
Thesis Co-Advisor

Robin Tokmakian
Thesis Co-Advisor

Peter Chu
Chair, Department of Oceanography

THIS PAGE INTENTIONALLY LEFT BLANK

ABSTRACT

Performance of the Navy's latest operational ocean forecast model (the Hybrid Coordinate Model, HYCOM, which became operational in March 2013) is systematically evaluated by comparing its velocity fields with actual ADCP velocities collected during a two-week cruise in the Agulhas Return Current region in 2012 (ARC 12). This chaotic region is complex and highly variable, with velocities sometimes exceeding 200 cm/s. Assessment using in-situ velocity measurements is very rare. This analysis characterizes the uncertainty in the model output and its predictions that Undersea Warfare operators, as well as other warfighters, obtain from the HYCOM output, and use in real world operations. Qualitative comparisons show good placement by HYCOM of persistent and energetic ocean current and eddy features, but difficulty (as expected, because HYCOM cannot resolve features finer than eddy scale) resolving the finer-scale variability present in the chaotic ARC region. Quantitative comparisons showed that the overall Root Mean Squared Error (RSME) is 35 cm/s and 47˚ near-surface, and 17 cm/s and 32˚ at 500 m depth, showing a general decrease of RMSE with depth.

THIS PAGE INTENTIONALLY LEFT BLANK

TABLE OF CONTENTS

LIST OF FIGURES

THIS PAGE INTENTIONALLY LEFT BLANK

LIST OF TABLES

THIS PAGE INTENTIONALLY LEFT BLANK

LIST OF ACRONYMS AND ABBREVIATIONS

ADCP	Acoustic Doppler Current Profiler
ARC	Agulhas Return Current
ARC12	Agulhas Return Current 2012 cruise
CTD	Conductivity Temperature Depth
DBDB2	Digital Bathymetry Data Base 2-minute resolution
ECMWF	European Centre for Medium-range Weather Forecasts
GDEM	Generalized Digital Environmental Model
GPS	Global Positioning System
HYCOM	HYbrid Coordinate Ocean Model
MICOM	Miami Isopycnal Coordinate Ocean Model
NAVGEM	Navy Global Environmental Model
NAVO	Naval Oceanographic Office
NCODA	Navy Coupled Ocean Data Assimilation
NCOM	Navy Coastal Ocean Model
NLOM	NRL Layered Ocean Model
NOGAPS	Navy Operational Global Atmospheric Prediction System
NRL	Naval Research Laboratory
RMSE	Root Mean Squared Error
R/V	Research Vessel
SSC	Stennis Space Center, MS
UNOLS	University-National Oceanographic Laboratory System
USW	Undersea Warfare
XBT	Expendable Bathythermeograph

THIS PAGE INTENTIONALLY LEFT BLANK

ACKNOWLEDGMENTS

Completion of this thesis would not have been possible without help and guidance from many people.

To Dr. Jeff Book, Dr. Mary Batteen and Dr. Robin Tokmakian: Thank you for your countless hours of guidance and assistance as advisors.

To Captain Rebecca Stone: Thank you for the foundation your numerical modeling class provided.

To Mr. Mike Cook: Thank you for your help with programming.

Additional thanks are owed to Dr. Ana Rice, Dr. Warren Wood and Mr. Joe Metzger of NRL Stennis Space Center, MS for their support in various phases of this work.

Most importantly, to my wife, Lindsey, and my son, Philip: Thank you for your patience, love, and support.

THIS PAGE INTENTIONALLY LEFT BLANK

I. INTRODUCTION

A. BACKGROUND

Given the relative scarcity of in-situ oceanic observations, there are only rare occasions for verification of ocean model output below the sea surface. Comparisons are more often made using remote sensing of surface features, not actual in-situ observations. When in-situ observations are available, they normally consist of temperature and salinity profiles with relatively poor horizontal resolution. Because in-situ velocity data are rarely available, data assimilation of in-situ velocity fields is not currently incorporated into operational ocean models.

The collection of Acoustic Doppler Current Profiler (ADCP) data on the Agulhas Return Current 2012 cruise (ARC12) during January and February 2012 allowed for a rare opportunity to make model-data comparisons of velocity fields. The cruise took place while the Naval Research Laboratory, Stennis Space Center, MS (NRL SSC) was still testing the HYbrid Coordinate Ocean Model (HYCOM), which had been chosen to become the Navy's newest operational ocean model by March 2013. HYCOM model output for the ARC12 cruise region, including velocity data, was made available to the ARC12 research team. Data collected during ARC12 included ADCP data, allowing for both qualitative and quantitative comparisons of HYCOM modeled velocities in the region of the Agulhas Return Current (ARC). The qualitative analysis gives a measure of the uncertainty in the model's representation of observed currents.

B. IMPORTANCE

Nearly every aspect of warfare is affected by the environment, but perhaps none more so than undersea warfare. Knowledge of the actual undersea environment can be crucial to the outcome of any operation. Prior to 1999, the best tool available to naval oceanographers for determining oceanic sound speed profiles was climatology from the Generalized Digital Environmental Model (GDEM; Teague et al. 1990). Made operational in 1999, the Modular Ocean Data Assimilation System (MODAS; Fox et al. 2002) was the first program to attempt a real time analysis, but provided no forecast capability. In 2006, the Navy Coastal Ocean Model (NCOM; Barron et al. 2006) became the first operational global ocean model, giving naval oceanographers the capability to make predictions about the undersea environment. HYCOM replaced NCOM in March 2013.

As Naval Oceanography continues to make more qualitative strides forward towards understanding the oceans, it is important to evaluate the effectiveness of new oceanographic tools as they become available. Of course, no analysis or prediction system is perfect, therefore every forecast has some degree of uncertainty. However, it is imperative to clearly understand the level of uncertainty in an analysis or forecast if that analysis or forecast will be subsequently used in operational decision making.

Understanding of HYCOM’s ability to characterize the battlespace environment will benefit the undersea warfare (USW) community, along with other warfighting disciplines. HYCOM will be used to make ocean predictions that will

drive decisions about naval operations across multiple warfare disciplines, but primarily in USW, where knowledge of the ocean environment is essential to successful operations. Equally crucial to that knowledge is understanding the uncertainty inherent in those analyses or predictions.

C. AGULHAS CURRENT SYSTEM

The Agulhas Current System, which is located along the east coast of Southern Africa, consists of the Agulhas Current, Agulhas retroflection, westward-drifting Agulhas rings spawned at the retroflection, and the eastward Agulhas Return Current (Figure 1). The system is fed primarily by recirculation of a southwest Indian Ocean subgyre to the east, with additional input from the north in the form of Mozambique Channel Eddies, and possibly some energy in the form of turbulent flow shed at the retroflection point of the East Madagascar Current (Lutjeharms 2007). A volume transport estimate made in the northern portion of the Agulhas Current was 69.7 +/- 4.3 Sv (Beal and Bryden 1999).

The ARC, which begins at the retroflection point and flows eastward, is the primary outflow from the Agulhas Current. Lutjeharms and Ansorge (2001) estimated the geostrophic volume transport in the upper 1500 m of the ARC across several sections near 21°E, with one section recording 54 Sv. This volume transport was deemed to be a representative middle value of their results.

The ARC makes a major meander equatorward as it passes over the Agulhas Plateau (Lutjeharms 2007). This meander creates a frequent spawning ground for eddies (Lutjeharms

and Valentine 1988). Continuing eastward, the ARC gradually loses strength until it finally merges into the South Indian Ocean Current between 66˚E and 70˚E (Lutjeharms and Ansorge 2001).

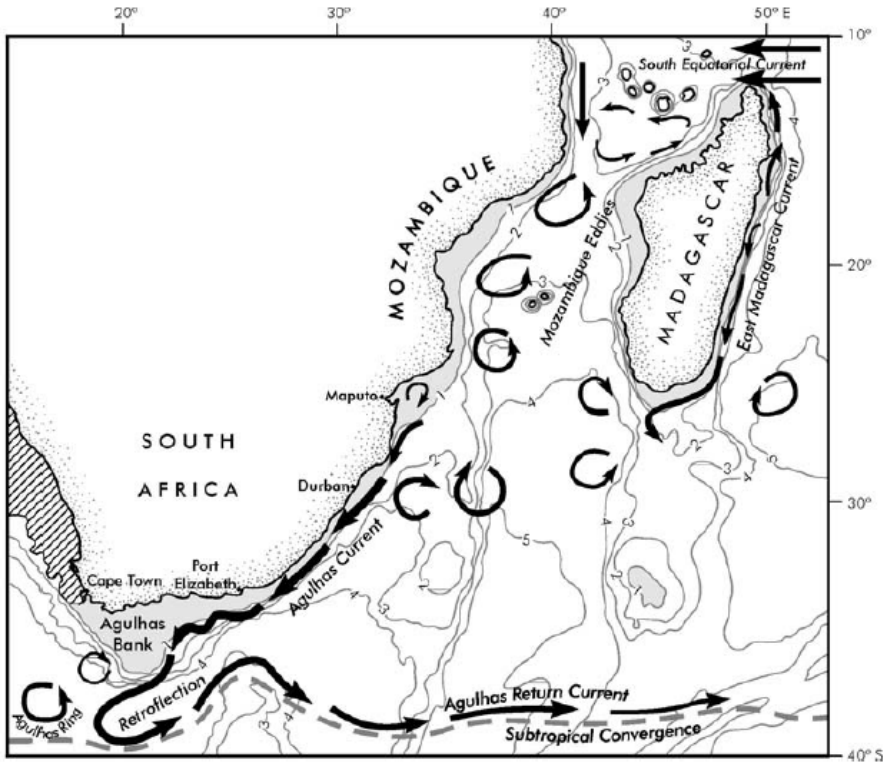

Figure 1. Greater Agulhas Current System (From Lutjeharms 2007).

D. AGULHAS RETURN CURRENT 2012 (ARC12) CRUISE

The ARC12 cruise began on 23 January 2012 and ended on 8 February 2012. The cruise was onboard R/V Melville, then the oldest operating research vessel in the University-National Laboratory System (UNOLS) fleet. Figure 2 shows the cruise track. ARC12 began and ended in Cape Town, South Africa, with the bulk of data being collected to the southeast in a box bound by 38˚S, 40˚S, 22˚E, and 26˚E.

The primary purpose of the cruise was to test the concept of seismic oceanography, a technique which uses low frequency sound pulses to identify strong temperature gradients in the ocean. "The project goals [were] to quantify physical processes of diapycnal mixing across a major ocean front with a focus on mesoscale eddy stirring and cross-frontal water mass exchange by making use of new acoustic methodology that provides high lateral resolution (order of 10 meters), full water column sections of isothermal fine-structure." (Wood, W. T. 2011, personal communication)

One should be aware that since the primary purpose of the cruise was not to collect ADCP data for model verification, the cruise track did not provide the perfect basis for comparison. One should also note, when interpreting the results of this study, that the cruise location was chosen for its strong and dynamic features. Therefore, one should not expect even an eddy-resolving ocean model, such as HYCOM, to reproduce conditions exactly as observed.

The remainder of this thesis will be organized as follows. Section II describes the ADCP data and the HYCOM model. Section III describes the methodology used in analyzing densely sampled ADCP velocity fields compared to gridded model output. Section IV describes the results, while Section V discusses the results. Section VI gives conclusions and offers suggestions on areas for future research.

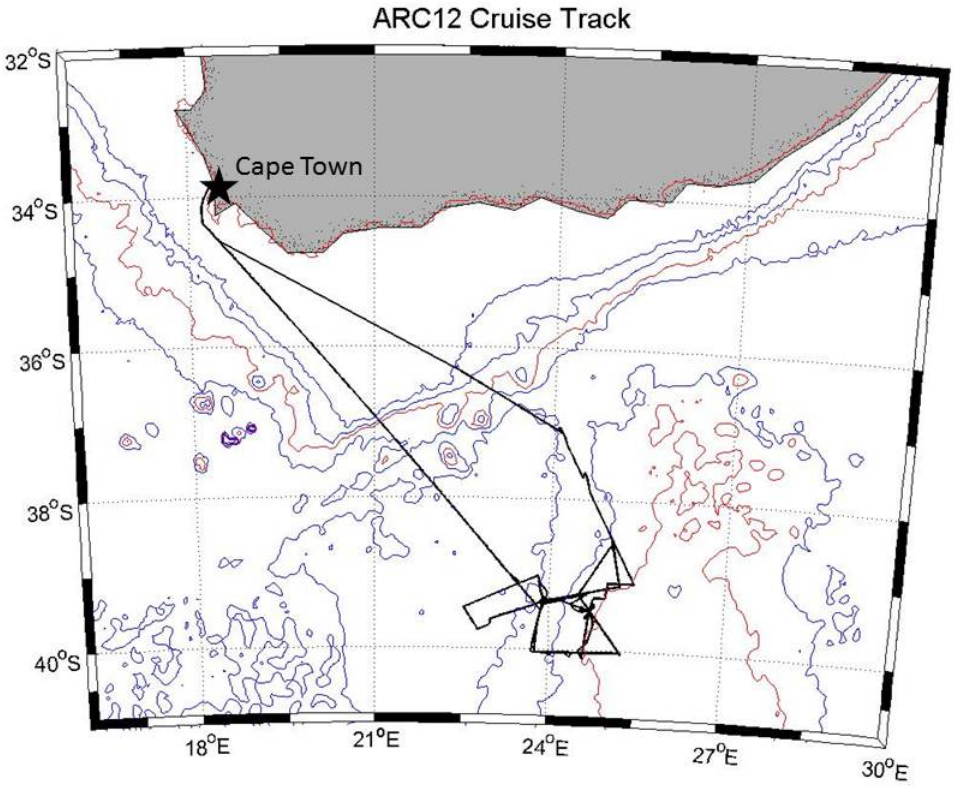

Figure 2. ARC 12 cruise track (black line) with DBDB2 bathymetry contours every 1000 meters. Red contour is 3000 meter curve.

II. DATA

This section will describe both the ADCP data collected on ARC 12 and the HYCOM model output, including a brief discussion of HYCOM's development and data assimilation scheme.

A. ADCP

R/V Melville is equipped with a Teledyne RD Instruments Ocean Surveyor ADCP, which has a typical velocity accuracy of ± 1% or ± 0.5 cm/s. The ADCP was operated near continuously for the duration of the underway period. Data were collected from 23 January to 8 February 2012. ADCP data were binned in 16 m increments from 29 m down to 973 m, for a total of 60 vertical levels.

The ADCP data set used in this thesis was processed using 5-minute averaging, which resulted in 4120 observations along the cruise track. Factoring in the vertical levels, over 200,000 points were sampled. Note that the ship speed was variable, which led to denser sampling in some regions as compared to others. For example, when Conductivity Temperature Depth (CTD) casts were made, over 20 ADCP observations could be recorded while the ship was nearly stationary. To avoid biases, such regions of oversampling were mostly, but not entirely, removed from comparisons.

In a few instances, ADCP data appeared not to accurately reflect the ocean environment. Reprocessing filtered most of the bad data points, but a few remained in the final data set and are suspected to have been caused by

bad Global Positioning System (GPS) data. To the maximum extent possible, these data points were removed, but it is possible that some were included in the final calculations.

B. HYCOM

1. History of U.S. Navy Operational Ocean Prediction

As stated earlier, prior to 1999, GDEM was the only tool a naval oceanographer had at his or her disposal to characterize ocean conditions where in-situ observations could not be obtained. Although GDEM's name suggests that it is a forecast model, it actually provides only climatology. In 1999, MODAS became operational. MODAS is capable of providing a global analysis by assimilating observation data.

The Global Ocean Forecast System version 2.5, which includes the NCOM model, the NRL Layered Ocean Model (NLOM), and MODAS, became the first operational global ocean model. The system was declared operational in 2006. At 0.12° to 0.17° resolution, NCOM was eddy permitting, meaning that it did not have the resolution to accurately model the behavior of major ocean eddies, but had sufficient resolution to show their existence. Higher resolution nested grid models were used in areas of interest. NCOM was used as the Navy's primary ocean forecasting tool inside the Global Ocean Forecast System until HYCOM was declared operational in March 2013.

2. Development of HYCOM

HYCOM's origins lie in the University of Miami's Miami Isopycnic Coordinate Ocean Model (MICOM) described in Bleck et al., 1992. Whereas a purely isopycnal vertical

coordinate system cannot adequately handle areas with no stratification or convective instability, the HYbrid Coordinate Model allows use of pressure coordinates (z-level) in areas where isopycnal coordinates would result in numerical instability. Bleck (2002) describes the coordinates and physics used in HYCOM. HYCOM was run in near-real time at Naval Research Laboratory, Stennis Space Center, MS (NRL SSC) beginning in 2006. HYCOM was delivered to the Naval Oceanographic Office (NAVO) and declared operational on 20 March 2013.

3. Model Characteristics

In its current configuration, HYCOM has a horizontal resolution of 0.08° and 32 vertical levels. The horizontal resolution enables HYCOM to resolve and model the behavior of major ocean eddies. The vertical levels can be isopycnals, pressure levels, or bottom-following sigma levels. The layered continuity equation is used for transitions between coordinate systems. Metzger et al. (2008) provides greater detail.

Initial conditions for the first HYCOM spin-up came from GDEM version 3.0. HYCOM then ran for 17 model years using forcing from the European Centre for Medium-range Weather Forecasting (ECMWF) reanalysis data. In real time, HYCOM currently uses the Naval Global Oceanographic Prediction System (NOGAPS) model for 3-hourly atmospheric forcing. Wind stress, air temperature, surface specific humidity, incoming/outgoing radiation and precipitation are input at 0.5° resolution (Metzger et al. 2008). HYCOM will transition to the Navy Global Environmental Model (NAVGEM) forcing when NOGAPS is retired in August 2013. HYCOM

bathymetry is provided by the NRL Digital Bathymetry Data Base 2-minute resolution (DBDB2).

4. Data Assimilation

HYCOM assimilates ocean observational data via the Naval Coupled Ocean Data Assimilation (NCODA) system. In order to maximize the benefit of late-arriving data (especially altimeter data), HYCOM begins the assimilation process with a hindcast run starting over 4 days prior to tau=0 initialization field valid time. During this hindcast, HYCOM assimilates five separate NCODA analyses using the timeline shown in Figure 3. Assimilation occurs incrementally over a 6-hour window. For each analysis, data are assimilated from +/- 36 hours for altimeter, -12 days to +12 hours for in-situ profiles, and +/- 12 hours for all other data, referenced to the start time of each assimilation window (described in Metzger et al. 2008 and modified in Metzger et al. 2010). Figure 4 is an example of how long altimeter data can take to be ingested into NCODA and illustrates how, if the only altimeter data used was for +/- 36 hours from tau zero, a large amount of data would arrive too late to ever be ingested into the model.

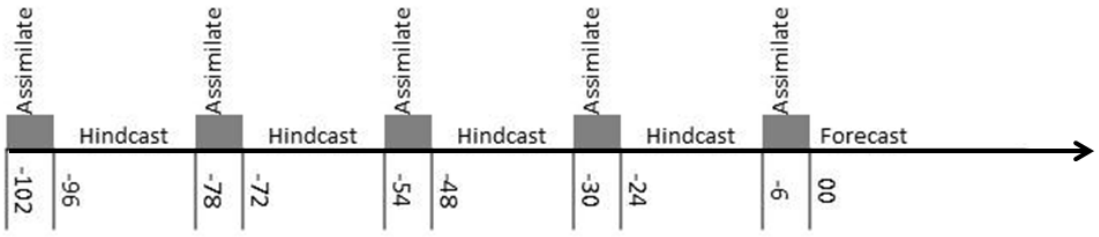

Figure 3. HYCOM/NCODA run stream. Numbers represent beginning and end times of assimilation window.

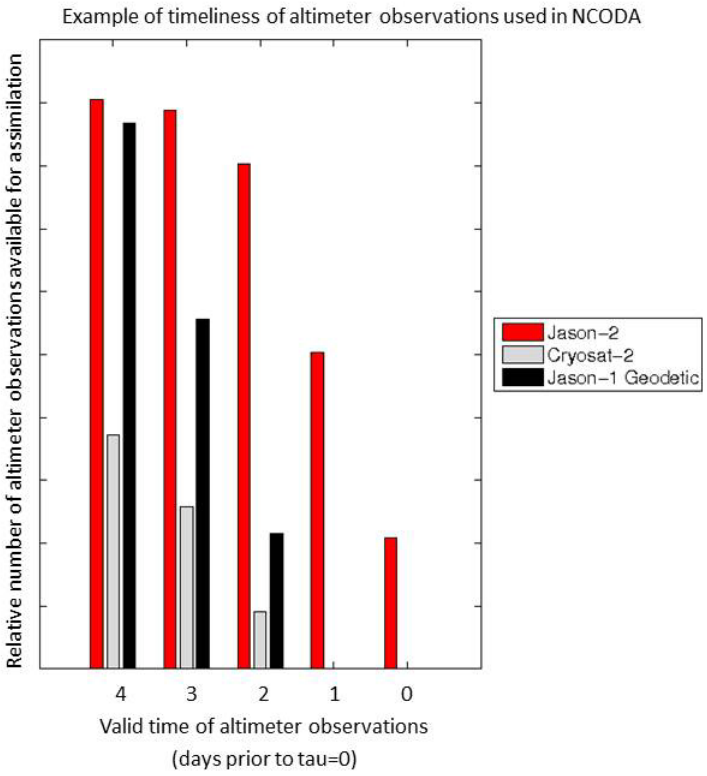

Figure 4. Example of altimeter observations available for assimilation into HYCOM-NCODA runstream (Based on E. J. Metzger 2013, personal communication).

5. Output

HYCOM initialization fields and 3-hourly forecasts from experiment 90.9 were provided for the period of the ARC-12 cruise. Model output from 2 and 4 February were missing, so 24- to 45-hour forecasts from 1 and 3 February were substituted. Model fields provided were temperature, salinity, sea surface height, and velocity. Horizontal resolution of the model output was 0.08 degrees and 40 vertical levels, post processed to constant depth surfaces. Vertical levels are described in Table 1. The area for the data was from 32.4˚S to 42.4˚S and 15.12˚E to 45.12˚E.

0	30	125	800
2	35	150	900
4	40	200	1000
6	45	250	1250
8	50	300	1500
10	60	350	2000
12	70	400	2500
15	80	500	3000
20	90	600	4000
25	100	700	5000

Table 1. Vertical levels of HYCOM output in meters.

III. METHODOLOGY

As this section will show, specific techniques were needed for comparing densely sampled 5-minute ADCP velocity observations with (relatively) coarsely gridded 3-hourly model output. Visual comparison techniques developed for this thesis enable easy comparisons and give a better understanding of the quality of the HYCOM modeled velocity fields.

A. INTERPOLATION

All data points are referenced to the time and location of the ADCP data collected along Melville's track. Data from HYCOM grid points were linearly and temporally interpolated to match the time, geographic location and depth for each ADCP data point, using the nearest four HYCOM grid points.

A comparison was initially attempted with no temporal interpolation; daily 00Z HYCOM model outputs were spatially interpolated and compared to ADCP data for 12-hours before and after the model valid time. This resulted in points along the track where the HYCOM values used for comparison shifted abruptly from one day's HYCOM analysis to another day's HYCOM analysis. Figure 4 illustrates the most severe case, where the HYCOM-modeled velocity jumped from 0.53 m/s in the 31 January initialization to 1.50 m/s in the 1 February initialization. For this very dynamic region, change is to be expected between model runs, but the extent of the change in this case was surprising.

Two JASON altimetry passes were made on 29 January in the ARC12 cruise region. Based on the timeline shown in Figure 4, it is possible those two altimetry passes had not yet been assimilated into the 31 January HYCOM/NCODA runstream, but were assimilated into the 01 February runstream. This change in data would account for the change shown in Figure 5. It is also possible, however, that either altimetry run was assimilated into both model runs or neither model run. Further analysis is required to determine whether timing of altimeter data assimilation was responsible for the change in initial conditions.

Given the significant temporal variability, 3-hourly forecasts were obtained for 03Z-21Z and, together with the 00Z analyses, were interpolated to match the observation time for each ADCP data point. An error caused HYCOM data not to be available for 02 and 04 February, so 24 through 45 hour forecasts from 01 and 03 February, respectively, were used as substitutes.

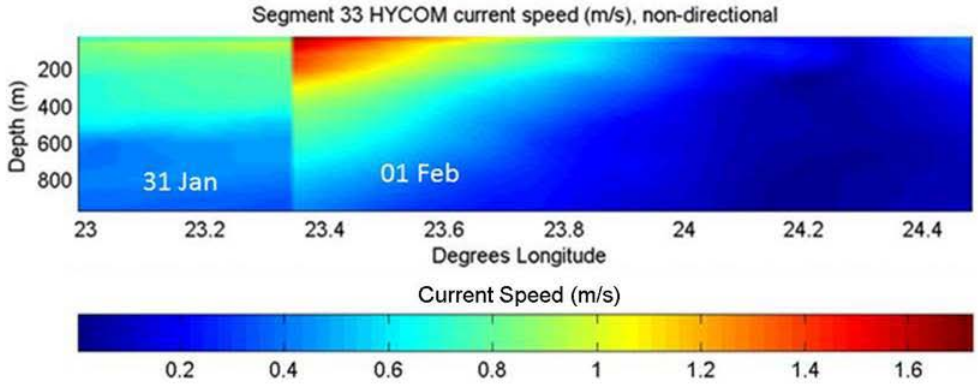

Figure 5. Jump discontinuity between uninterpolated model runs.

B. COMPARISON

1. Segments Used

For model-data comparison, the cruise track (which, as Figure 2 shows, could have significant changes in ship track direction) was divided into segments so as to create a monotonic relationship between sample time and either latitude or longitude. This criterion would allow for easy plotting of either a depth vs. longitude or depth vs. latitude velocity cross section, depending on a segment's orientation. Using only this criterion, many segments were plotted that covered very little distance. Those segments were later discarded, but the original numbering system (segments from 1 to 52) was kept for sake of continuity. Table 2 gives positional data for the actual segments analyzed, as well as beginning and end times for the segments. Some segments include turns, so the representative track is not necessarily a straight line between the start and stop locations. Also, note that segment length is not uniform; therefore error statistics cannot be equally weighted for each segment. Furthermore, spacing of data points along segments is not spatially uniform, as each point represents five minutes of averaged data, which could cover a variable distance based on ship's speed. This resulted in some over-sampling during periods of slow speed. Whenever possible, segments were truncated to minimize this over sampling. As a result, not all ADCP data collected during ARC12 were used in this comparison.

Seg.#	Start Position		Time/Date (2012)		End Position		Time/Date (2012)		# Pts.
1	36.319˚ S	22.401˚ E	20:16	24-Jan	37.119˚ S	24.116˚ E	5:05	25-Jan	110
3	37.054˚ S	24.076˚ E	8:55	25-Jan	37.710˚ S	24.505˚ E	20:20	25-Jan	140
5	37.644˚ S	24.540˚ E	22:35	25-Jan	39.078˚ S	25.430˚ E	13:13	26-Jan	167
6	39.094˚ S	25.416˚ E	13:52	26-Jan	39.095˚ S	25.004˚ E	15:15	26-Jan	21
7	39.097˚ S	24.987˚ E	15:37	26-Jan	39.294˚ S	24.963˚ E	16:16	26-Jan	15
8	39.297˚ S	24.947˚ E	16:52	26-Jan	39.296˚ S	24.764˚ E	17:17	26-Jan	11
9	39.303˚ S	24.751˚ E	17:47	26-Jan	40.110˚ S	24.591˚ E	23:23	26-Jan	72
10	40.110˚ S	24.591˚ E	23:47	26-Jan	39.429˚ S	24.704˚ E	5:05	27-Jan	67
11	39.469˚ S	24.675˚ E	8:57	27-Jan	39.474˚ S	24.712˚ E	13:13	27-Jan	60
15	39.474˚ S	24.511˚ E	21:12	27-Jan	39.430˚ S	24.407˚ E	3:03	28-Jan	76
18	39.391˚ S	24.382˚ E	5:52	28-Jan	39.247˚ S	24.634˚ E	8:08	28-Jan	35
19	39.259˚ S	24.539˚ E	13:12	28-Jan	39.396˚ S	23.871˚ E	21:21	28-Jan	103
20	39.378˚ S	23.866˚ E	21:57	28-Jan	39.137˚ S	25.199˚ E	16:16	29-Jan	219
21	39.135˚ S	25.204˚ E	16:12	29-Jan	38.484˚ S	25.023˚ E	3:03	30-Jan	140
23	38.746˚ S	25.098˚ E	6:57	30-Jan	38.565˚ S	25.064˚ E	15:15	30-Jan	107
24	38.558˚ S	25.059˚ E	15:52	30-Jan	39.363˚ S	23.908˚ E	5:05	31-Jan	160
25	39.365˚ S	23.897˚ E	5:12	31-Jan	39.105˚ S	23.816˚ E	8:08	31-Jan	46
26	39.098˚ S	23.814˚ E	9:02	31-Jan	39.364˚ S	23.891˚ E	11:11	31-Jan	33
27	39.367˚ S	23.898˚ E	11:47	31-Jan	39.025˚ S	23.806˚ E	14:14	31-Jan	37
28	39.019˚ S	23.798˚ E	14:52	31-Jan	39.459˚ S	22.525˚ E	0:00	1-Feb	112
33	39.629˚ S	22.989˚ E	8:47	1-Feb	39.265˚ S	24.481˚ E	23:23	1-Feb	176
34	39.266˚ S	24.488˚ E	23:27	1-Feb	40.010˚ S	25.225˚ E	12:12	2-Feb	154
35	40.016˚ S	25.222˚ E	12:17	2-Feb	40.036˚ S	23.716˚ E	6:06	3-Feb	223
36	40.033˚ S	23.709˚ E	6:52	3-Feb	39.356˚ S	23.905˚ E	16:16	3-Feb	117
37	39.349˚ S	23.914˚ E	16:37	3-Feb	39.324˚ S	24.272˚ E	20:20	3-Feb	50
38	39.324˚ S	24.273˚ E	20:47	3-Feb	39.327˚ S	24.129˚ E	0:00	4-Feb	49
39	39.327˚ S	22.126˚ E	0:52	4-Feb	39.438˚ S	24.554˚ E	2:02	4-Feb	24
41	39.472˚ S	24.699˚ E	5:52	4-Feb	39.575˚ S	24.617˚ E	8:08	4-Feb	27
43	39.459˚ S	24.714˚ E	9:12	4-Feb	39.519˚ S	24.679˚ E	11:11	4-Feb	30
44	39.527˚ S	24.684˚ E	11:42	4-Feb	40.038˚ S	25.258˚ E	17:17	4-Feb	67
45	40.017˚ S	25.107˚ E	19:57	4-Feb	40.032˚ S	24.074˚ E	5:05	5-Feb	116
47	40.046˚ S	24.066˚ E	8:32	5-Feb	40.033˚ S	23.761˚ E	12:12	5-Feb	44
48	40.025˚ S	23.760˚ E	12:12	5-Feb	39.350˚ S	23.860˚ E	17:17	5-Feb	68
51	39.470˚ S	23.852˚ E	0:22	6-Feb	39.027˚ S	23.330˚ E	5:05	6-Feb	63
52	39.036˚ S	23.345˚ E	5:37	6-Feb	37.003˚ S	21.089˚ E	5:05	7-Feb	285

Table 2. Location and time data for each segment beginning and end, with total number of data points for each segment shown in the far right column.

2. Qualitative Comparison

HYCOM and ADCP vector near-surface (29 m depth) velocities were plotted for each segment along the track for visual speed and direction comparison. Vector comparisons were made primarily at this near-surface level, but cross-sections were also plotted to compare current speed changes between the surface and 900 m depth. Each segment was inspected to note similarities and differences in current magnitude and direction. Due to the variability between HYCOM runs observed in Figure 4, overlapping segments were analyzed to determine ADCP-observed temporal variability. Because, as stated earlier, the cruise was not primarily focused on collecting ADCP data for model verification, the cruise track did not provide the perfect basis for comparison. In particular, fewer overlapping segments were made than would have been ideally desired for this comparison. Nevertheless, four separate transects of ocean were sampled at least twice, giving a sufficient basis for comparison.

3. Quantitative Comparison

Numerical comparisons were made first by comparing Root Mean Squared Error (RMSE) of HYCOM-modeled speed and direction versus the ADCP-sensed speed and direction. Some segments (e.g., segment 4) along the full cruise track were discarded due to oversampling or bad data. As a result, all calculations include only data from the particular segments listed in Table 2. Invariably, a few of these tracks contained missing or bad data, so data for these points were interpolated from adjacent points.

RMSE was calculated for each segment for the following levels: near-surface, 100 m and 500 m. Near surface uses the uppermost ADCP depth bin, or 29 m depth. Note that ADCP depth bins are uniformly spaced, while HYCOM output level spacing increases with depth. Therefore, looking at just these three levels gives a more realistic picture of HYCOM's performance than considering all 60 ADCP bin levels for which statistics were calculated. Near surface uses the uppermost ADCP depth bin, or 29-m.

RMSE was calculated for speed and direction using Equation 1 (where F is the modeled value, A is the observed value, and n is the total number of data points):

$$RMSE = \sqrt{\sum_{i=1}^{n} \frac{(F-A)^2}{n}} \quad (1)$$

Note that since raw speed RMSE statistics tend to favor low-energy regions where differences are slight, and penalize high energy regions where differences are numerically large (but smaller in scale compared to the velocities actually observed), a weighted RMSE was calculated for speed using Equation 2:

$$Weighted\_RMSE = \sqrt{\sum_{i=1}^{n} \frac{\left[(F-A)/A\right]^2}{n}} \quad (2)$$

IV. RESULTS/ANALYSIS

A. OVERALL

Table 3 shows the RMSE for each segment of the cruise. Overall speed and direction RMSE for HYCOM on all segments were 0.34 m/s and 43.4˚ near the surface, with error decreasing to 0.18 m/s and 28.9˚ at 500 m depth.

Note that figures in this section show either 1) multiple ADCP observations of segments covering similar geographic transects (e.g., Figure 6) or 2) comparisons of ADCP and HYCOM data for a single segment (e.g., Figure 7). In all cases, the upper figure shows near-surface (29 m depth) velocity vectors, with the 0.5 m/s standard vector shown in the bottom left corner of the graphic. Note that the vector scale is fixed to the geographic scale of each plot; therefore the length of the standard velocity vector in plots with different spatial limits is scaled differently. Each vector plot shows the grid points for which HYCOM data are produced. A grid point model such as HYCOM requires at least 4 grid points to resolve a feature and 7 to 8 grid points to properly model a feature. The presence of model grid points on each plot will allow for interpretation of whether local minima and maxima or major direction changes are spatially too small to be captured or modeled by HYCOM.

The lower half of each figure shows either a depth-longitude or depth-latitude cross section (based on the direction the segment was sampled) of current speed. Note that the speed is non-directional for all plots. In cases where HYCOM output is compared to ADCP data, HYCOM output

always appears below the ADCP data. The velocity color scale used in all cross-sectional plots is either from 0 to 1 m/s or 0 to 2 m/s. Velocities exceeding the maximum value of the color scale are shown in black.

In many plots, the ADCP will observe a feature that HYCOM does not model in the same geographic location. The Appendix contains additional figures showing a broader view of HYCOM's analysis for each day of the cruise, which can be used to determine whether differences between ADCP and HYCOM output were due to spatial errors in HYCOM's placement of a feature.

	Weighted speed RMSE			Speed RMSE (m/s)			Direction RMSE (degrees)		
Seg.#	Surface	100-m	500-m	Surface	100-m	500-m	Surface	100-m	500-m
1	104.7%	50.4%	53.5%	0.38	0.21	0.18	90.73	95.85	87.77
3	**47.2%**	**37.2%**	**31.4%**	**0.23**	**0.16**	**0.16**	**23.38**	**13.43**	**10.41**
5	56.0%	38.9%	58.0%	0.18	0.17	0.19	31.90	13.91	30.51
6	50.3%	70.1%	17.6%	0.78	0.22	0.07	20.65	29.42	11.21
7	40.5%	57.4%	11.6%	0.16	0.18	0.03	57.86	53.79	7.81
8	57.6%	12.1%	20.9%	0.72	0.04	0.07	36.64	35.33	7.80
9	**98.7%**	**85.7%**	**73.7%**	**0.40**	**0.33**	**0.21**	**82.52**	**73.68**	**61.39**
10	156.8%	118.5%	131.5%	0.38	0.39	0.22	81.97	72.73	62.90
11	41.3%	54.9%	55.2%	0.21	0.30	0.17	42.68	48.89	9.55
15	18.0%	25.3%	55.1%	0.10	0.10	0.14	25.94	29.79	17.51
18	332.4%	108.3%	26.9%	0.37	0.29	0.05	108.32	48.49	10.33
19	**60.9%**	**57.4%**	**31.1%**	**0.25**	**0.23**	**0.06**	**25.87**	**35.41**	**35.06**
20	**108.6%**	**111.0%**	**59.4%**	**0.26**	**0.28**	**0.13**	**52.70**	**29.34**	**42.26**
21	65.7%	66.4%	30.8%	0.23	0.22	0.07	41.85	46.95	10.92
23	145.4%	106.9%	46.8%	0.35	0.30	0.10	36.27	7.02	6.55
24	**504.6%**	**121.0%**	**233.6%**	**0.34**	**0.27**	**0.09**	**57.63**	**34.08**	**48.02**
25	**59.5%**	**25.7%**	**36.4%**	**1.04**	**0.34**	**0.21**	**30.79**	**31.26**	**35.33**
26	50.8%	42.1%	45.9%	0.92	0.59	0.27	26.67	28.35	23.59
27	49.5%	28.8%	44.4%	1.03	0.36	0.28	14.57	30.04	20.54
28	115.3%	31.6%	19.8%	0.35	0.14	0.12	28.31	22.18	10.41
33	**43.9%**	**43.7%**	**44.3%**	**0.54**	**0.39**	**0.24**	**69.92**	**58.13**	**39.63**
34	**30.2%**	**38.8%**	**47.4%**	**0.22**	**0.29**	**0.26**	**25.14**	**16.19**	**12.82**
35	**46.6%**	**32.9%**	**42.4%**	**0.37**	**0.22**	**0.20**	**26.89**	**12.68**	**13.05**
36	**208.5%**	**56.2%**	**46.5%**	**0.41**	**0.17**	**0.11**	**40.82**	**21.63**	**33.91**
37	**69.5%**	**53.4%**	**42.2%**	**0.67**	**0.23**	**0.11**	**100.41**	**104.68**	**66.66**
38	28.5%	106.0%	58.2%	0.07	0.08	0.05	134.02	67.33	68.63
39	42.7%	31.0%	16.6%	0.24	0.13	0.04	37.37	26.07	37.16
41	18.6%	26.6%	11.5%	0.24	0.35	0.06	3.15	1.29	4.91
43	18.3%	32.5%	15.4%	0.24	0.46	0.09	4.94	4.12	8.36
44	**38.1%**	**54.3%**	**65.2%**	**0.29**	**0.36**	**0.32**	**78.85**	**90.84**	**16.96**
45	**35.1%**	**37.8%**	**46.3%**	**0.39**	**0.31**	**0.26**	**31.60**	**23.29**	**26.28**
47	100.5%	75.5%	47.9%	0.23	0.15	0.07	27.55	39.50	22.56
48	**188.0%**	**120.6%**	**50.1%**	**0.24**	**0.21**	**0.06**	**63.91**	**37.21**	**50.32**
51	**39.6%**	**18.0%**	**22.8%**	**0.37**	**0.23**	**0.14**	**44.14**	**41.97**	**41.25**
52	69.4%	70.9%	45.2%	0.38	0.32	0.33	62.24	64.81	46.56
All	98.6%	61.7%	52.6%	0.35	0.26	0.17	47.41	38.47	31.92

Table 3. RMSE values by segment. Results for bolded segments will be discussed.

B. COMPARISONS ALONG REPEATED TRACKS

To better understand the variability along the ARC12 cruise track, several repeat tracks were analyzed. Four geographic track lines were closely repeated by at least two segments of ARC12. Four east-west oriented segments were completed in the same geographic area along the eastern front of the Agulhas Return Current. Two northwest-southeast oriented segments and two east-west segments captured a southward jet of current in a warm core eddy. Another comparison was made between a pair of north-south oriented segments run just south of the Agulhas Return Current.

Observations made in each set of repeating segments revealed the naturally occurring temporal variability of the features present, which was compared to the modeled variability. Significant variation was observed. However, observed variation was still far less than the jump discontinuity shown in the HYCOM output in Figure 5.

1. Eastern Front of Agulhas Return Current

R/V Melville completed five tracks in the vicinity of 39.4˚S, 23.9˚E between 28 January and 3 February. These tracks are segments 19, 20, 24, 33, and 38 in Tables 2 and 3. Segment 20 was not used for this comparison as its data within the overlapping region was collected on the same day as segment 19. Segment 20 will be discussed separately. The upper section of Figure 6 shows the variation in near-surface velocities over this time period. Note that features in Figure 6 change rapidly over 1 to 2 grid points. For example, on segment 33 between 23.9˚E and 24.1˚E, flow changes from northeastward at almost 2 m/s to

southeastward at less than 0.2 m/s. Also note the eastward progression of the Agulhas Return Current, as it is barely visible in the cross-section on 28 January and then shifts eastward approximately 0.05˚ each two-day period between repeating segments. Within the overlapping region, the peak velocity recorded during segment 19 was 0.79 m/s, which increased to 1.37 m/s and 1.89 m/s by the time segments 24 and 33, respectively, were completed.

To better understand the variability, average near-surface velocities were calculated for the regions where all four segments overlapped by taking the average u and v velocities. Table 4 shows these values. The $2*\sigma$ (where σ is defined as the standard deviation) values of the average speeds and directions are shown to quantify the extent of natural variability observed among overlapping portions of the four segments. Note that the overlapping area of the tracks does not include most of the high-velocity Agulhas Return Current flow observed along the majority of segment 33; therefore the variability shown in Table 4 should not be mistaken as a representation of variability in the magnitude and direction of the high energy flow in the core of the ARC.

Date (Segment)	28-Jan (19)	30-Jan (24)	1-Feb (33)	3-Feb (37)	2*σ
Speed (m/s)	0.50	0.13	0.44	0.47	0.34
Direction	9.41˚	46.46˚	51.16˚	70.87˚	51.38

Table 4. Average velocities observed between 23.9E and 24.3E along segments 19, 24, 33 and 37, with second standard deviation for speed and direction values.

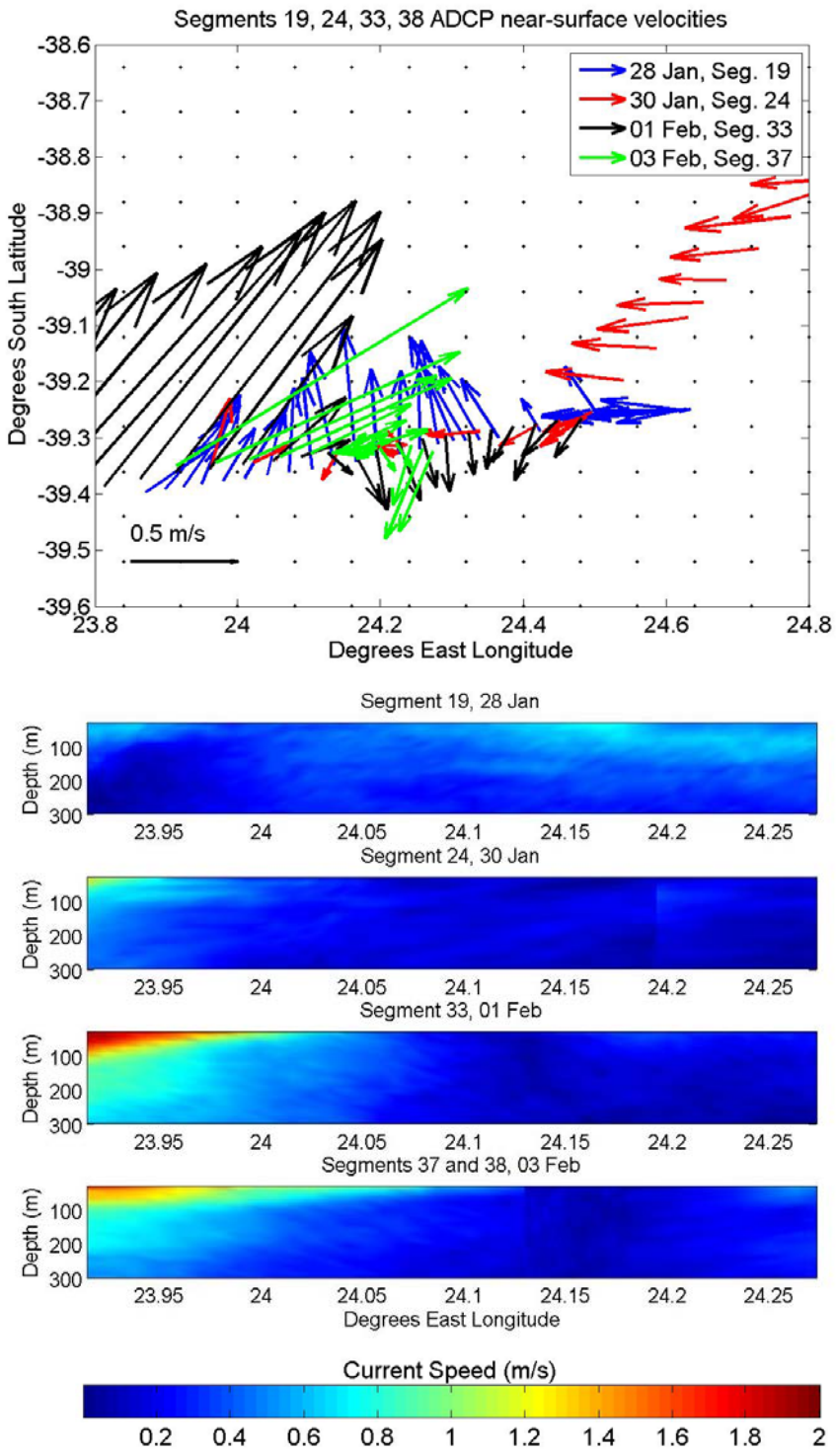

Figure 6. Change in velocities observed near 39.4˚S, 23.9˚E from 28 January to 3 February. Upper subfigure shows near-surface ADCP velocity vectors, lower subfigures show depth-longitude ADCP speed cross sections.

a. Segment 19, 28 January

Segment 19, shown in Figure 7, was 32.4 nm long and included 103 ADCP data points, with every 3rd velocity vector plotted. The westward extent of this segment barely began to capture the northward flow of the Agulhas Return Current. In the ADCP data, northward velocities of up to 0.79 m/s were observed and the average velocity was 0.22 m/s. HYCOM placed the bulk of the energy for this segment well east of its observed location, and did not capture the increase in speed at the western end of the segment, where the edge of the Agulhas Return Current was observed. Note that significant fluctuations occurred at the sub-grid scale level, such as the velocity maxima and minimum near 24.2˚E and 24.3˚E.

b. Segment 24, 30 and 31 January

Segment 24, seen in Figure 8, was 78.5 nm long and included 160 ADCP data points with an average observed velocity of 0.19 m/s, with every 4th point plotted. One of the most striking observations that can be made for segment 24 is that HYCOM depicted higher than observed velocities for nearly every single point along the track. HYCOM only had a positive bias for 6 segments, whose combined number of samples accounted for 17% of the overall cruise track. Analysis of additional model output reveals that HYCOM placed the northwest edge of a warm core eddy within segment 24. The positive velocity bias may have been a result of HYCOM placing the eddy slightly west of its actual location. Direction between HYCOM and ADCP was relatively consistent, except for the area just east of the western end of the track. The edge of the ARC appeared at

the far western end of segment 24 in the ADCP data. The transition from minimal velocity to strong northward flow was rather abrupt, with flow transitioning from near zero to a 1.37 m/s northward flow over a distance of less than two HYCOM grid points at 24.0˚E on the track. By contrast, the HYCOM analysis depicted in Figure 8 showed the eastward edge of the current at approximately 24.2˚E and a broad area of northward flow extending well east of the ADCP observed edge, which was west of 24.0˚E.

c. Segment 33, 1 February

Segment 33, shown in Figure 9, was 73.7 nm long and contained 176 ADCP data points, with every 5th point plotted. This segment captured a well-defined cross section of the Agulhas Return Current, with a maximum observed velocity of 1.98 m/s and average observed velocity of 0.58 m/s. Note that the HYCOM depiction of the current placed the eastern edge 0.6˚ west of the ADCP observed location. Also of interest, maximum velocities in the current core were observed near the eastern edge of the current. The transition from nearly 2 m/s to almost no current happened over the distance of less than two model grid points. By only considering the points in segment 33 west of 24.05˚E, in the northeastward flow of the Agulhas Return Current, the direction RMSE was reduced from the values show in Table 3 to 8.7˚ near surface, 12.1˚ at 100 meters, and 4.4˚ at 500 meters. Speed RMSE showed little change because HYCOM placed peak velocities near 23.2˚E and decreasing toward the 24.0˚E edge of the current, whereas the ADCP observed velocities of nearly 2 m/s right up to the edge of the current.

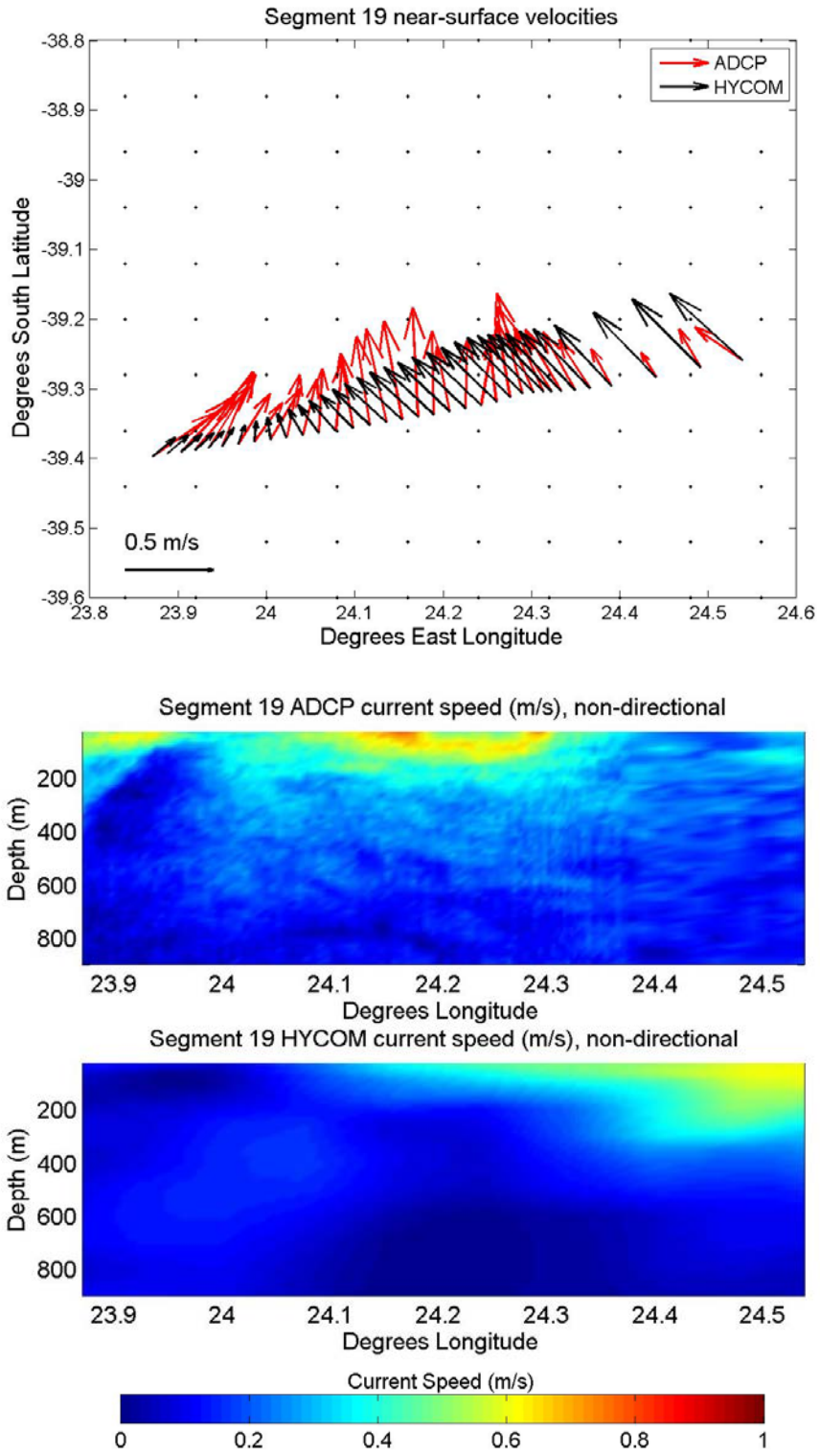

Figure 7. Segment 19 HYCOM and ADCP velocities. Near-surface velocities shown on top, ADCP velocity cross section in middle, and HYCOM velocity cross section at bottom.

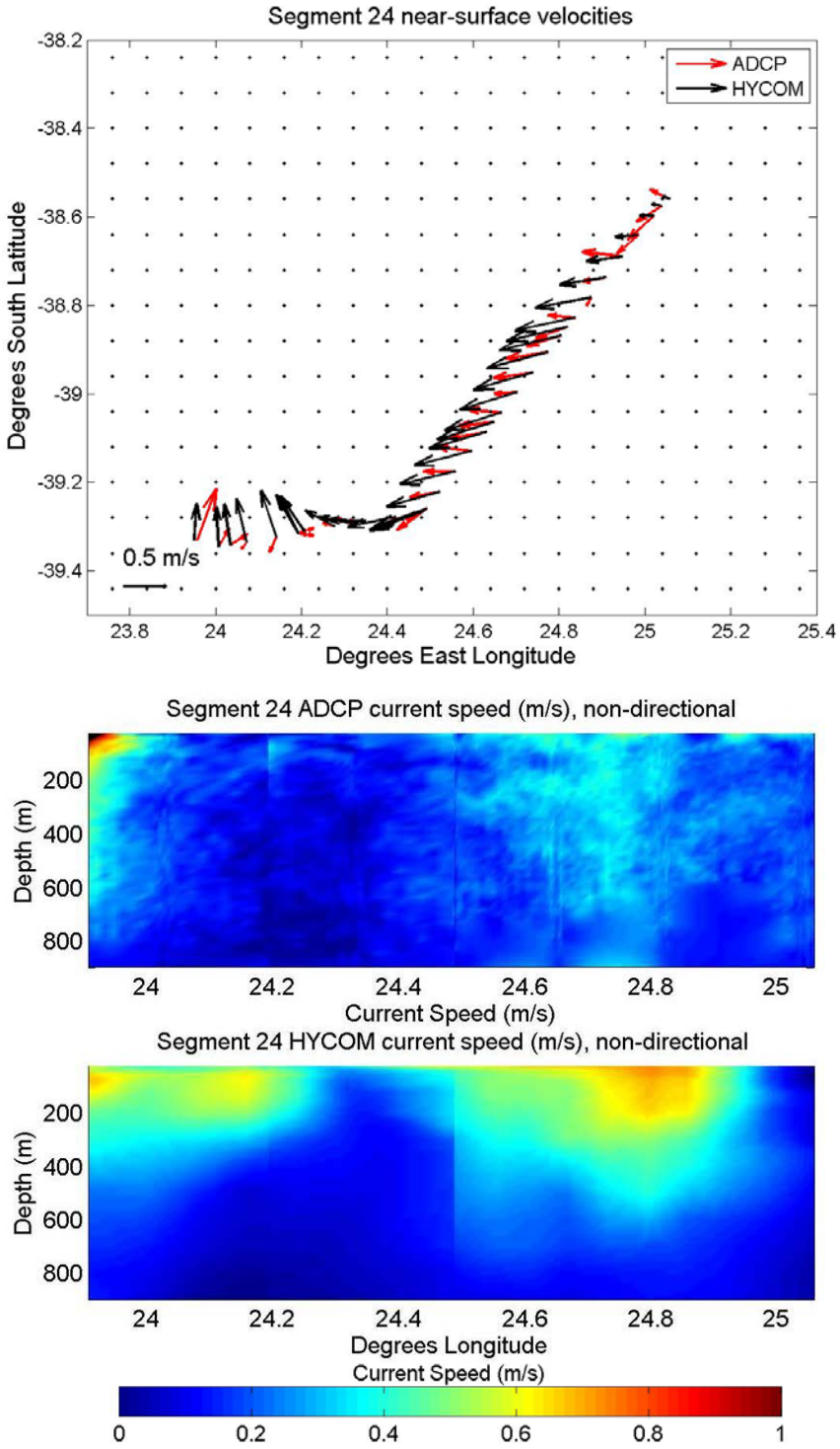

Figure 8. Segment 24 HYCOM and ADCP velocities. Near-surface velocities shown on top, ADCP velocity cross section in middle, and HYCOM velocity cross section at bottom. Velocities greater than 1 m/s are shown in black.

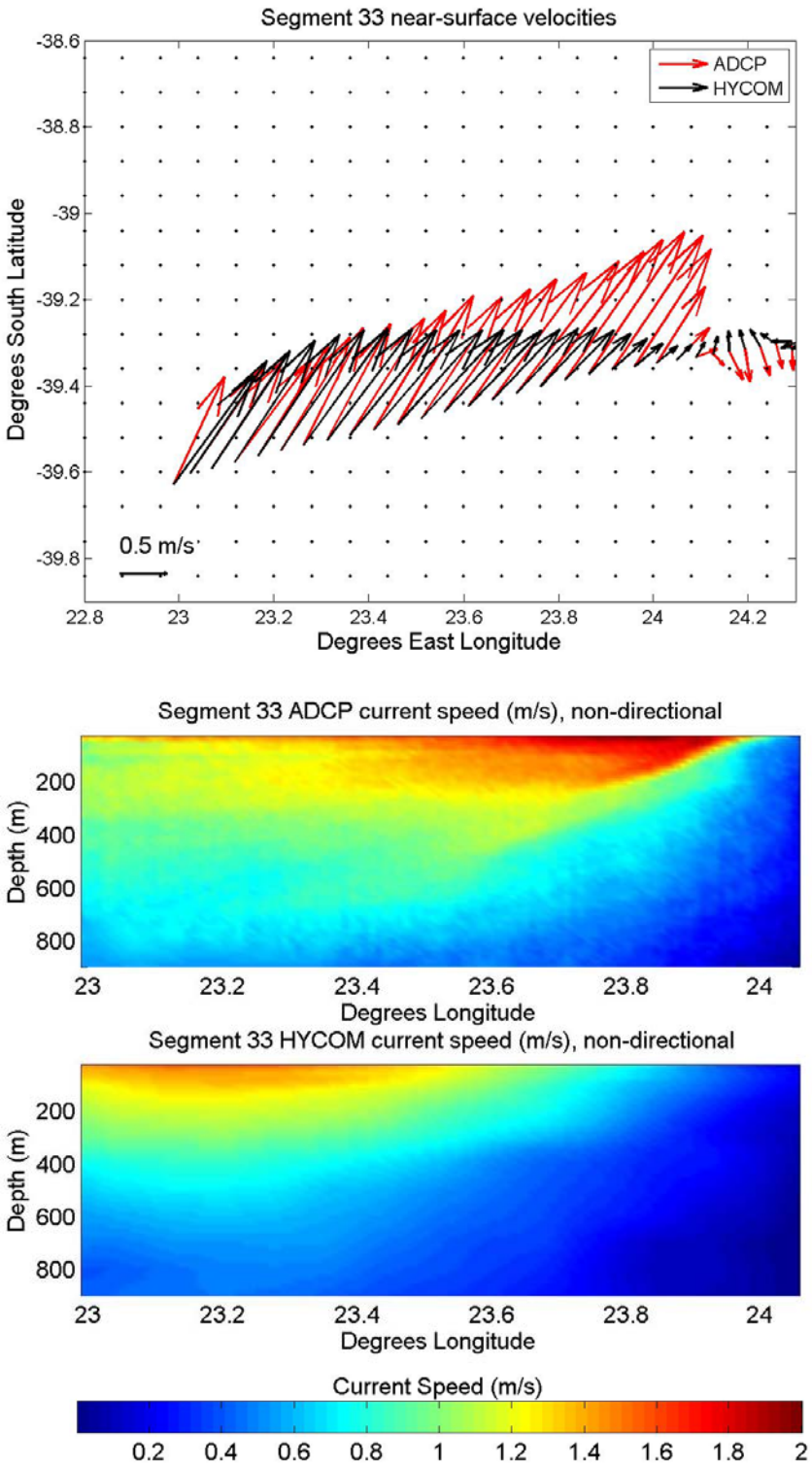

Figure 9. Segment 33 HYCOM and ADCP velocities. Near-surface velocities shown on top, ADCP velocity cross section in middle, and HYCOM velocity cross section at bottom.

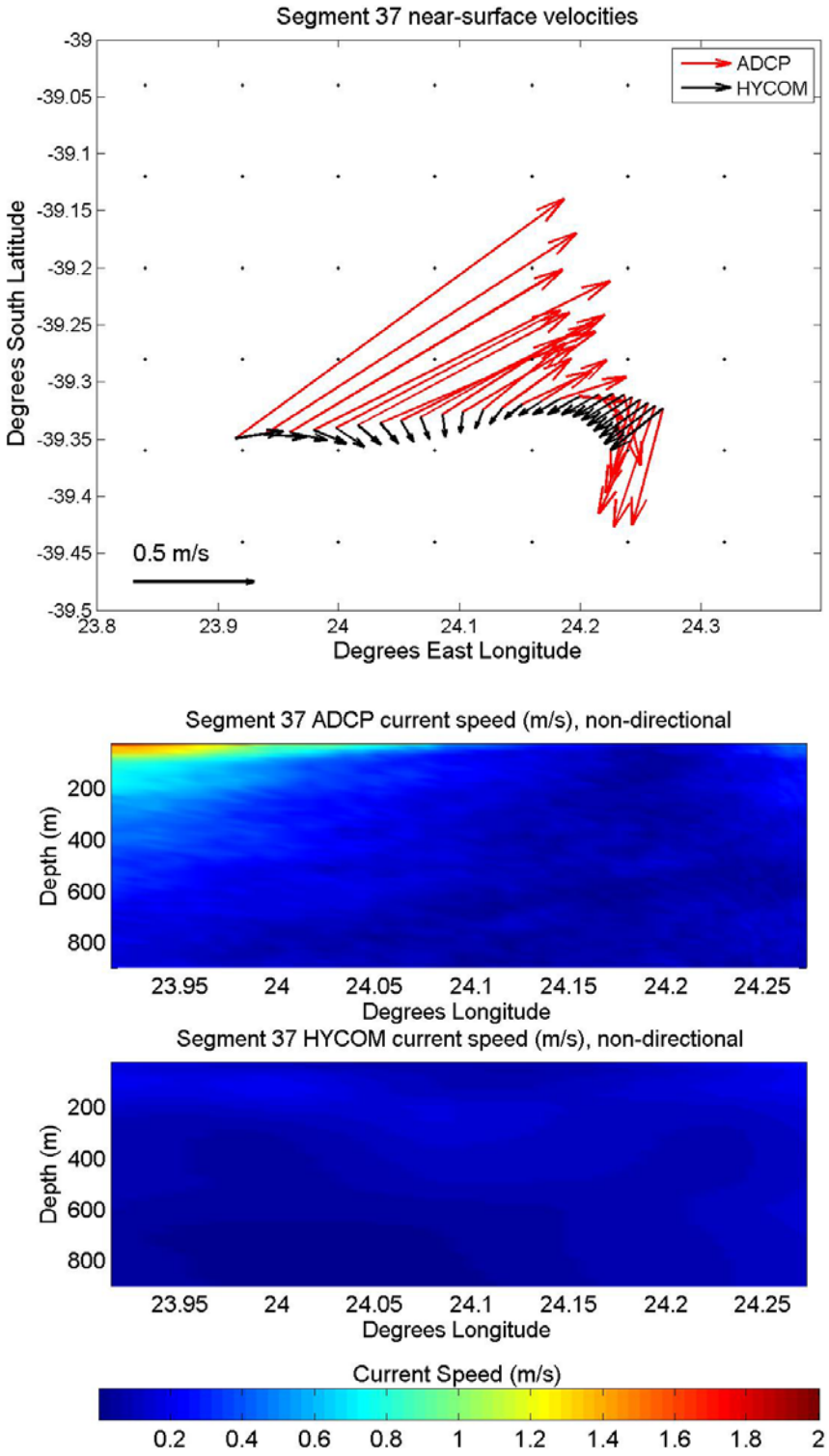

Figure 10. Segment 37 HYCOM and ADCP velocities. Near-surface velocities shown on top, ADCP velocity cross section in middle, and HYCOM velocity cross section at bottom.

d. Segment 37, 3 February

Segment 37, with an average velocity of 0.20 m/s, was a relatively short segment at only 17.6 nm and containing 50 ADCP data points. Every other velocity vector is shown in Figure 10. Note the rapid transition at the edge of the ARC, where near-surface speeds increased to 1.72 m/s in 1-2 grid points. Note also that HYCOM did not show the ARC at these locations on this day. An analysis of the full HYCOM velocity field for this time (Figure 36) showed the current placed farther west.

2. Comparisons of Warm Core Eddy velocities

Two overlapping transects were made along a northwest-southeast track passing near 39.6˚S, 24.8˚E on 2 and 4 February. These tracks, labeled segments 34 and 44, crossed a radius of a warm core eddy with currents flowing towards the southwest (Book et al., 2012). The eddy maintained a relatively constant location and shape during the time period between transects. A comparison of the two transects is depicted in Figure 11. The vector comparison, in particular, shows great similarity in near-surface current structure. Unfortunately, segment 44 did not start as far to the northwest as segment 34, but did cover enough of the eddy radius to make a relatively good comparison for the center and southeastern portions of segment 34. Both the vector and cross section plots in Figure 11 indicate a significant speed increase between 2 and 4 February. During this time period, maximum observed speeds increased from 1.11 m/s on 2 February to 1.53 m/s on 4 February.

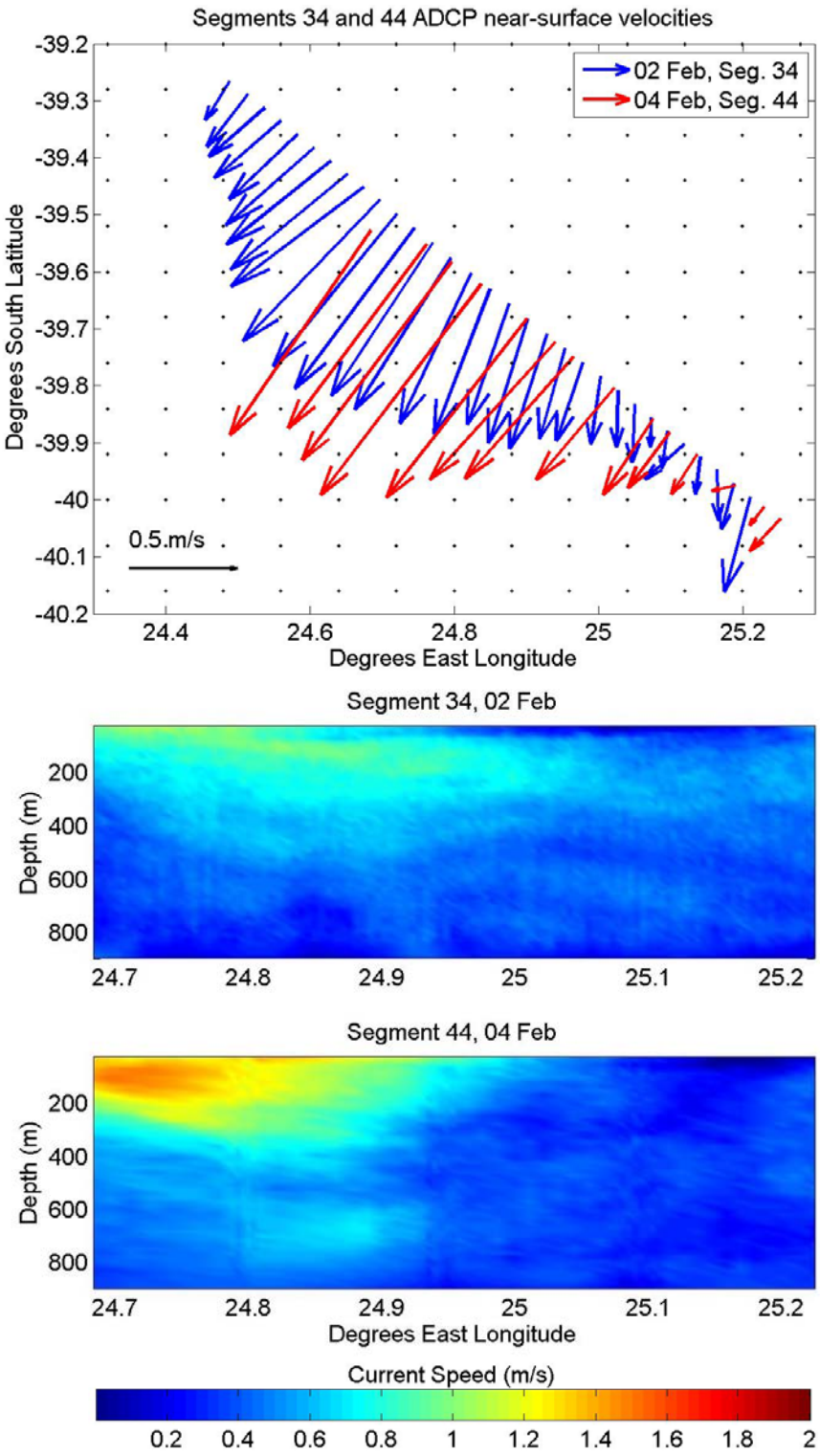

Figure 11. Change in velocities observed near 39.6˚S, 24.8˚E from 2 to 4 February. Upper subfigure shows near-surface ADCP velocity vectors, lower subfigures show depth-longitude ADCP speed cross sections.

a. Segment 34, 2 February

With 154 ADCP data points along a 56.5 nm track, segment 34, shown in Figure 12, was well sampled. The currents in this segment had an average observed velocity of 0.49 m/s, with a maximum of 1.11 m/s. Velocity vectors shown in Figure 12 were thinned to every 4th vector. The same figure's cross sectional plot shows that HYCOM placed the current core reasonably well, but did not capture the full strength of the current. HYCOM also consistently depicted the flow direction more westerly than was observed.

b. Segment 44, 4 February

Segment 44 repeats much of the ground covered by segment 34, although over a slightly shorter 41.6 nm segment with only 67 ADCP sampling points. Figure 13 depicts the near-surface velocity vectors (thinned to every other vector) and a cross section of the current. The average velocity along the track was 0.56 m/s. Maximum velocity was 1.53 m/s, a significant increase over segment 34's observed maximum. Although HYCOM continued to show weaker flow than observed, it did show that speed increased since 2 February. The depth of the eastern section of current core was less than observed, but the maximum speeds were well placed, and flow direction throughout the entire current was consistent with observations. The eastern edge of the segment, where weak flow was observed, was not simulated by HYCOM nearly as well as the rest of the segment. Removing this portion from calculations dropped the near-surface direction RMSE to only 13.0˚.

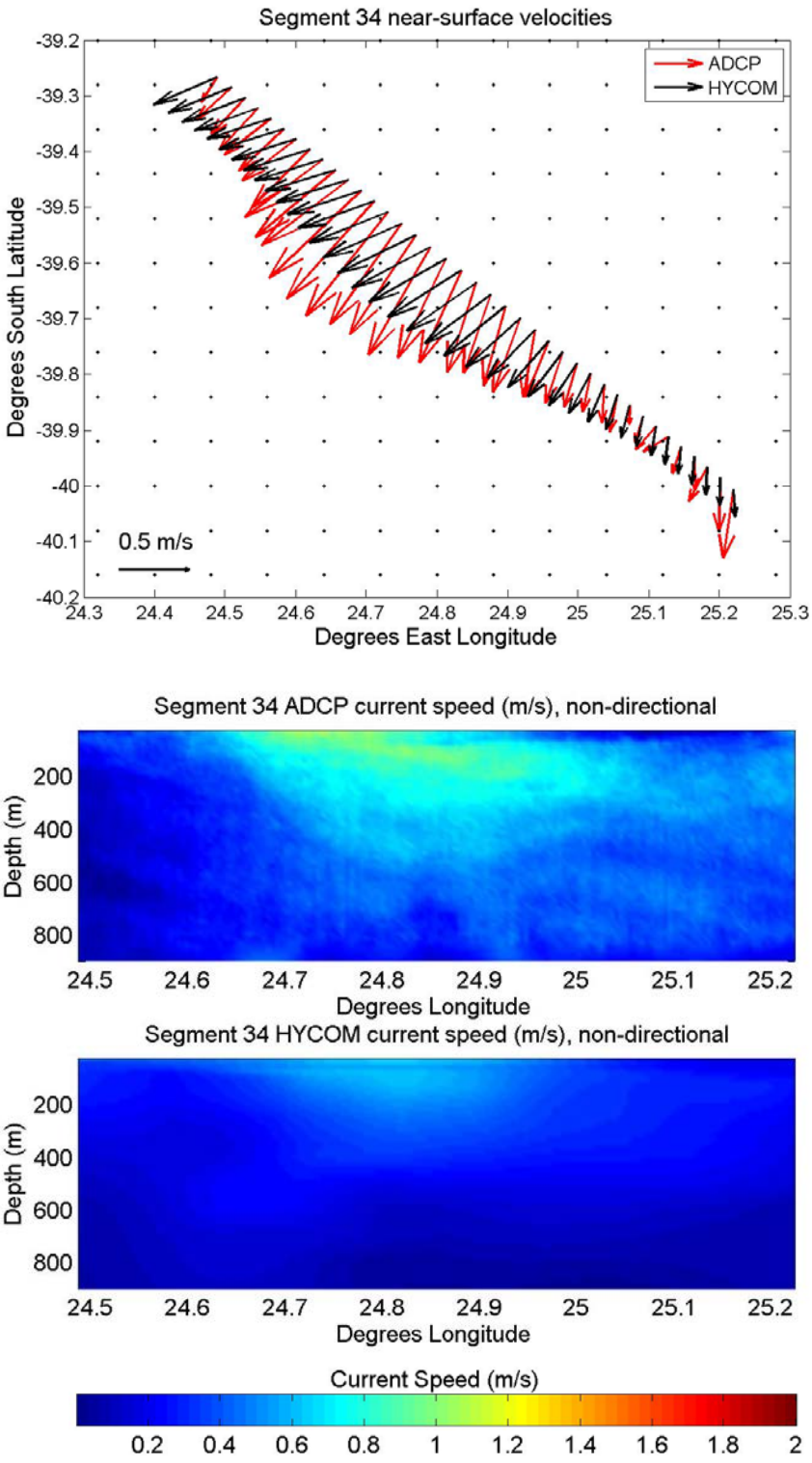

Figure 12. Segment 34 HYCOM and ADCP velocities. Near-surface velocities shown on top, ADCP velocity cross section in middle, and HYCOM velocity cross section at bottom.

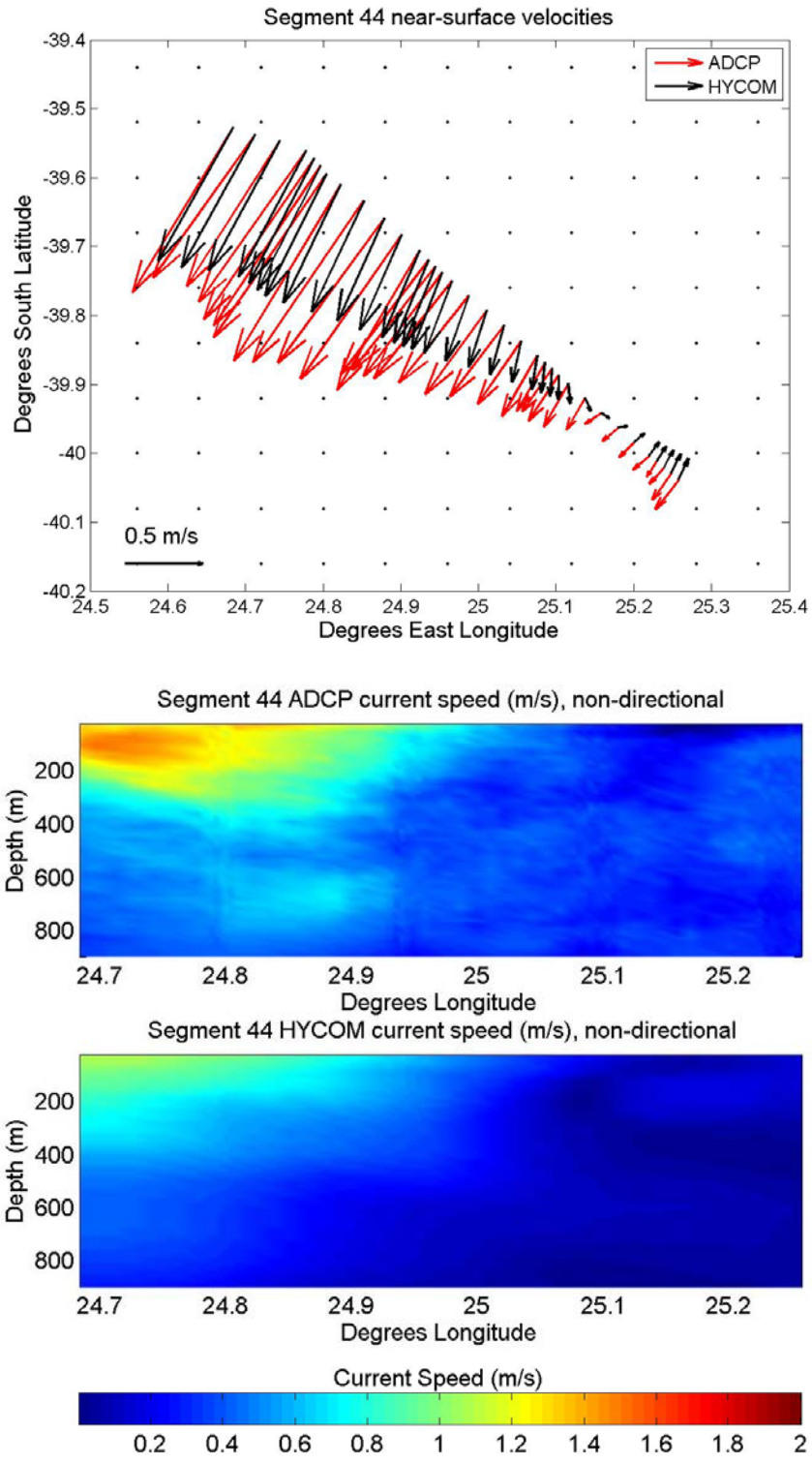

Figure 13. Segment 44 HYCOM and ADCP velocities. Near-surface velocities shown on top, ADCP velocity cross section in middle, and HYCOM velocity cross section at bottom.

3. Comparisons of Warm Core Eddy velocities

ADCP Segments 35 and 45 (compared in Figure 14) sampled the same warm core eddy depicted in Figures 11-13, but this time going from the center of the eddy out to its western edge. Segment 35 was recorded 2 and 3 February, and Segment 45 on 4 and 5 February. One will immediately note that very little changed over the 2-day period. Overall maximum and average velocities recorded in both segments were nearly identical. One significant difference to note is that Segment 45 recorded slightly higher core current speeds at depths between 50 and 400 meters. Near-surface speeds and directions were very similar along both tracks.

a. Segment 35, 1 and 2 February

Segment 35 was a 69.7 nm track which included 223 ADCP data points. The segment's maximum observed velocity was 1.42 m/s, with an average of 0.53 m/s. Both the vector (every 5th shown) and cross-sectional views in Figure 15 show that HYCOM captured the shape of the current with reasonable accuracy, but depicted a narrower and weaker feature than was actually observed. HYCOM underforecasted the strength observed in the current core, with a maximum modeled velocity of only 0.95 m/s. The western edge of the current was well depicted, but the eastern edge was placed about 0.4° west of its observed location. HYCOM did, however, capture the higher velocities between 400 and 600 meters near 24.6°E as shown in the longitude-depth plots of Figure 15.

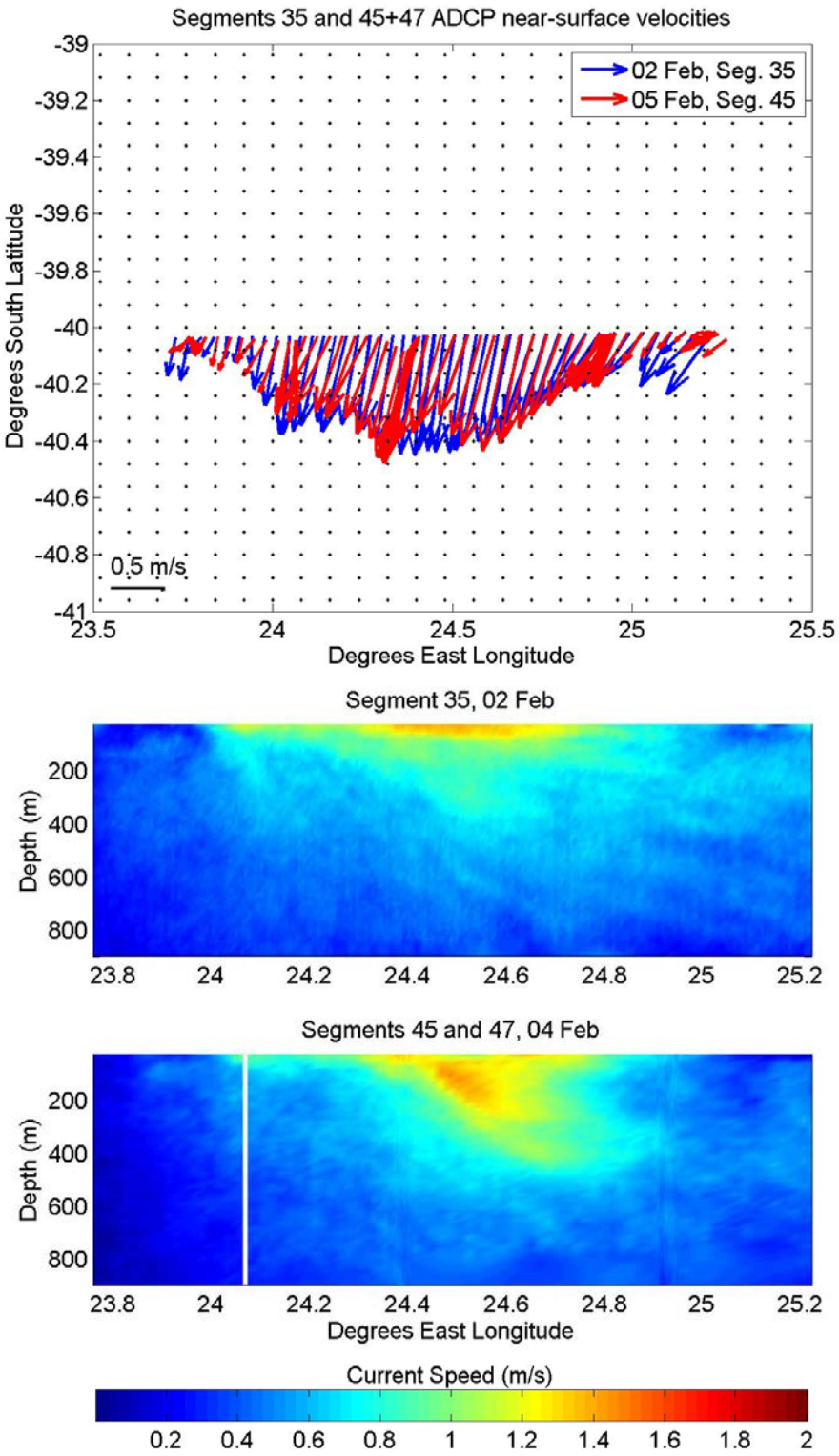

Figure 14. Change in velocities observed near 40.0˚S, 24.5˚E from 2 to 4 February. Upper subfigure shows near-surface ADCP velocity vectors, lower subfigures show depth-longitude ADCP speed cross sections.

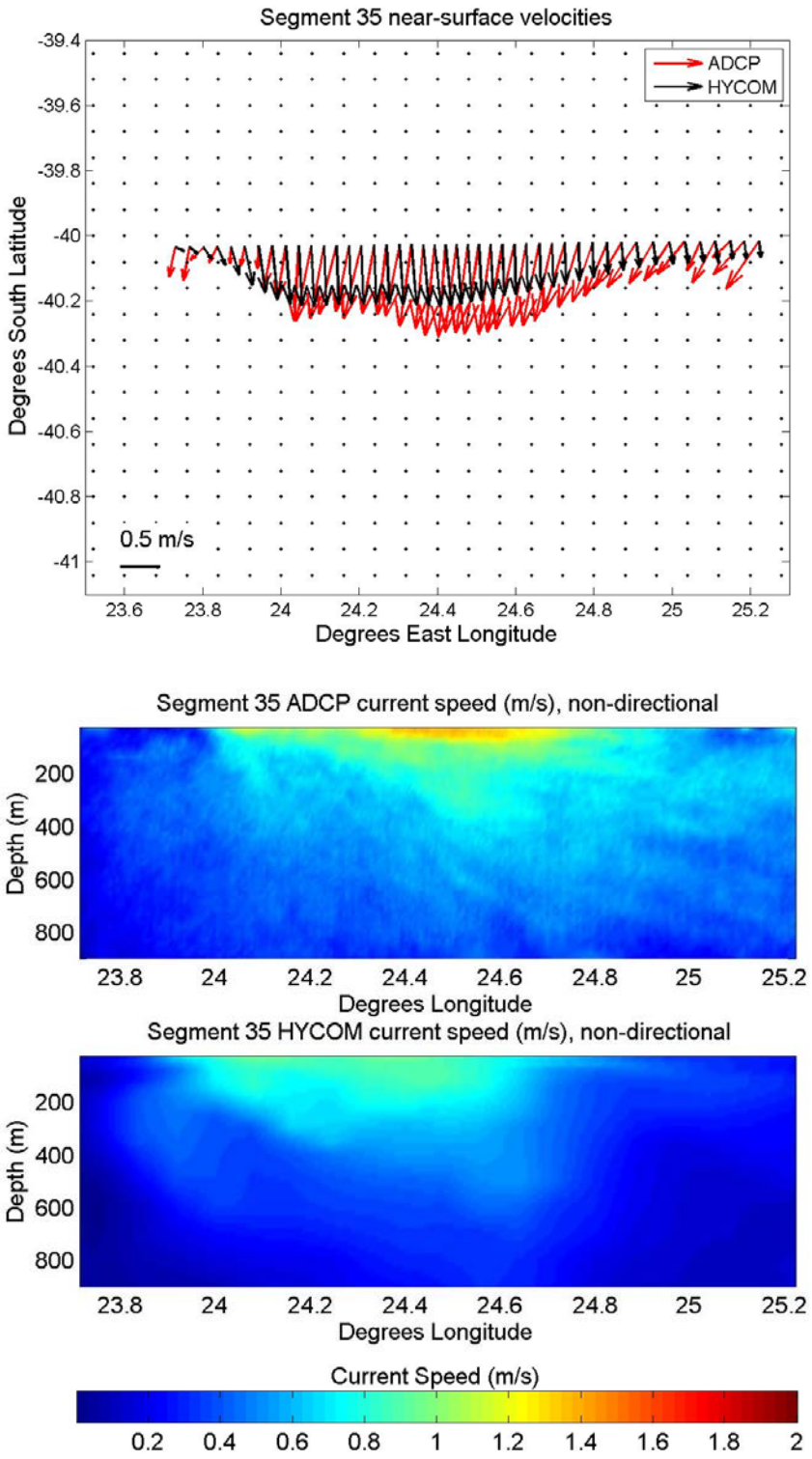

Figure 15. Segment 35 HYCOM and ADCP velocities. Near-surface velocities shown on top, ADCP velocity cross section in middle, and HYCOM velocity cross section at bottom.

b. Segment 45, 3 and 4 February

Segment 45 consisted of 116 ADCP data points along a 51.8 nm westward track. Velocities observed were very similar to those observed on segment 35, with a maximum of 1.46 m/s and an average of 0.59 m/s. ADCP vectors depicted in Figure 16 were thinned to every 3rd data point. The figure shows the comparison of ADCP to model velocities along the track. This segment included two CTD casts where the ship drifted slowly with the current. Those casts, done near 24.4˚E and 25.0˚E, resulted in some oversampling, as is apparent from the closeness of the velocity vectors at those locations. Nevertheless, the differences at these locations were representative of the differences observed along the entire segment, so data from those points were included the statistics given in Table 3. In the cross-sectional comparison, it is noteworthy that HYCOM accurately models the below-surface shape of the current, including the stronger below-surface currents observed at 24.7˚E. HYCOM still underestimated the strength of the current. Note that when comparing Figures 15 and 16 the temporal changes in HYCOM output between 2 and 4 February were very similar to the ADCP observed temporal changes.

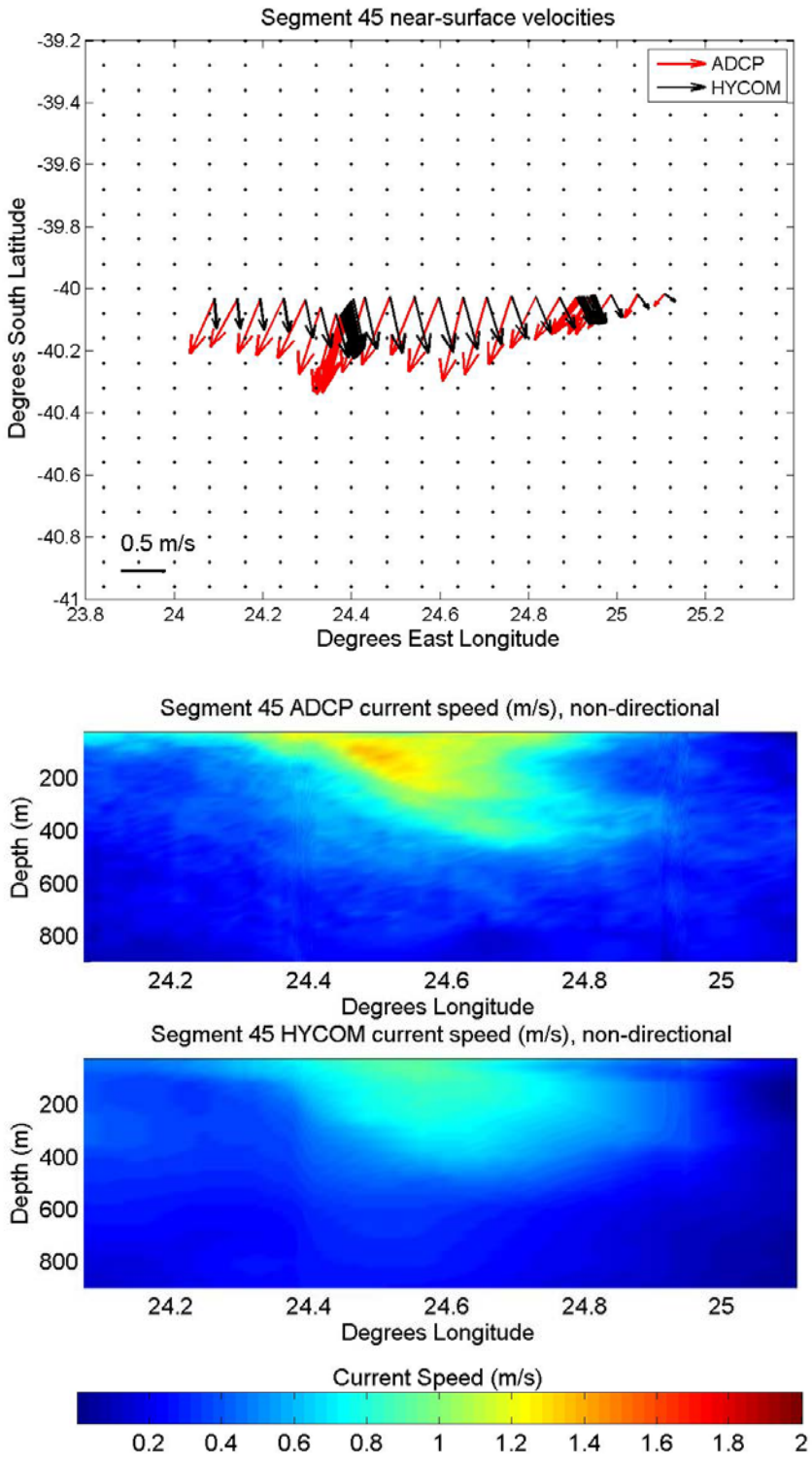

Figure 16. Segment 45 HYCOM and ADCP velocities. Near-surface velocities shown on top, ADCP velocity cross section in middle, and HYCOM velocity cross section at bottom.

4. South Front of Agulhas Return Current

The northern extents of both segments 36 and 48 just began to include the ARC near 39.4˚S 23.8˚E. Segment 36 was recorded on 3 February, and segment 48 on 5 February. Maximum observed velocities decreased on 5 February, but the placement of the ARC's southern edge was similar. Figure 17 shows a comparison between ADCP observations taken on the two segments.

a. Segment 36, 3 February

Most of the 117 ADCP data points along the 42.0 nm track of segment 36 (Figure 18) recorded very little energy, giving an average velocity of only 0.20 m/s. The maximum velocity, observed at the northern end of the track, was 1.60 m/s. This high-energy flow was part of the ARC, but HYCOM did not place any part of the ARC within this segment and depicted no velocities greater than 0.23 m/s. As a result of this mismatch, near surface HYCOM and ADCP velocities in Figure 18 compare poorly at the northernmost two grid points. This comparison shows how easily a small shift in model placement of a feature can result in poor error statistics, especially over a relatively small sample area. Examination of the full HYCOM velocity field in Figure 36 shows that HYCOM placed the ARC 0.1˚ west of segment 36 on 3 February.

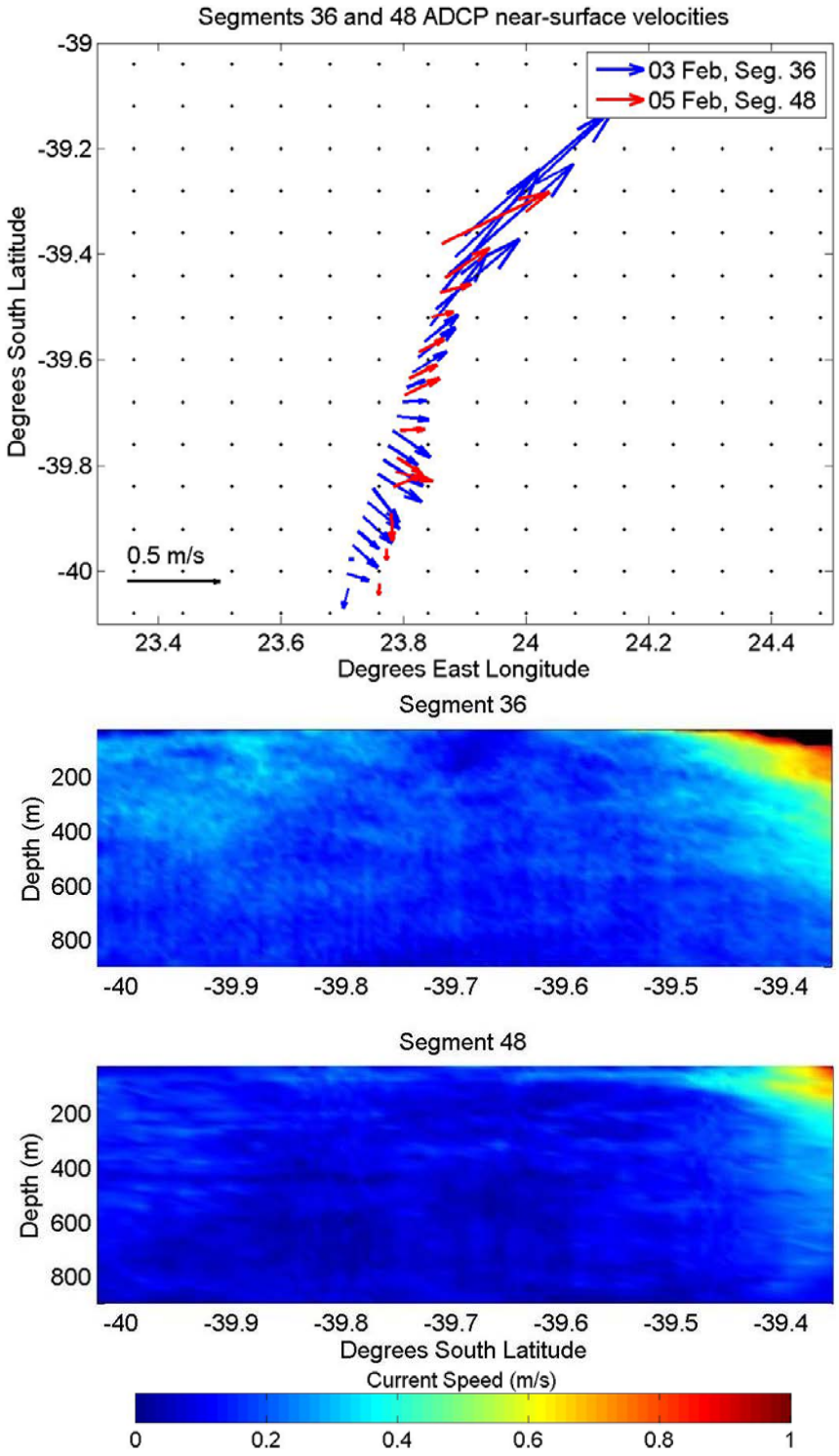

Figure 17. Change in velocities observed near 39.5˚S, 23.8˚E from 3 to 5 February. Upper subfigure shows near-surface ADCP velocity vectors, lower subfigures show depth-longitude ADCP speed cross sections. Velocities greater than 1 m/s are shown in black.

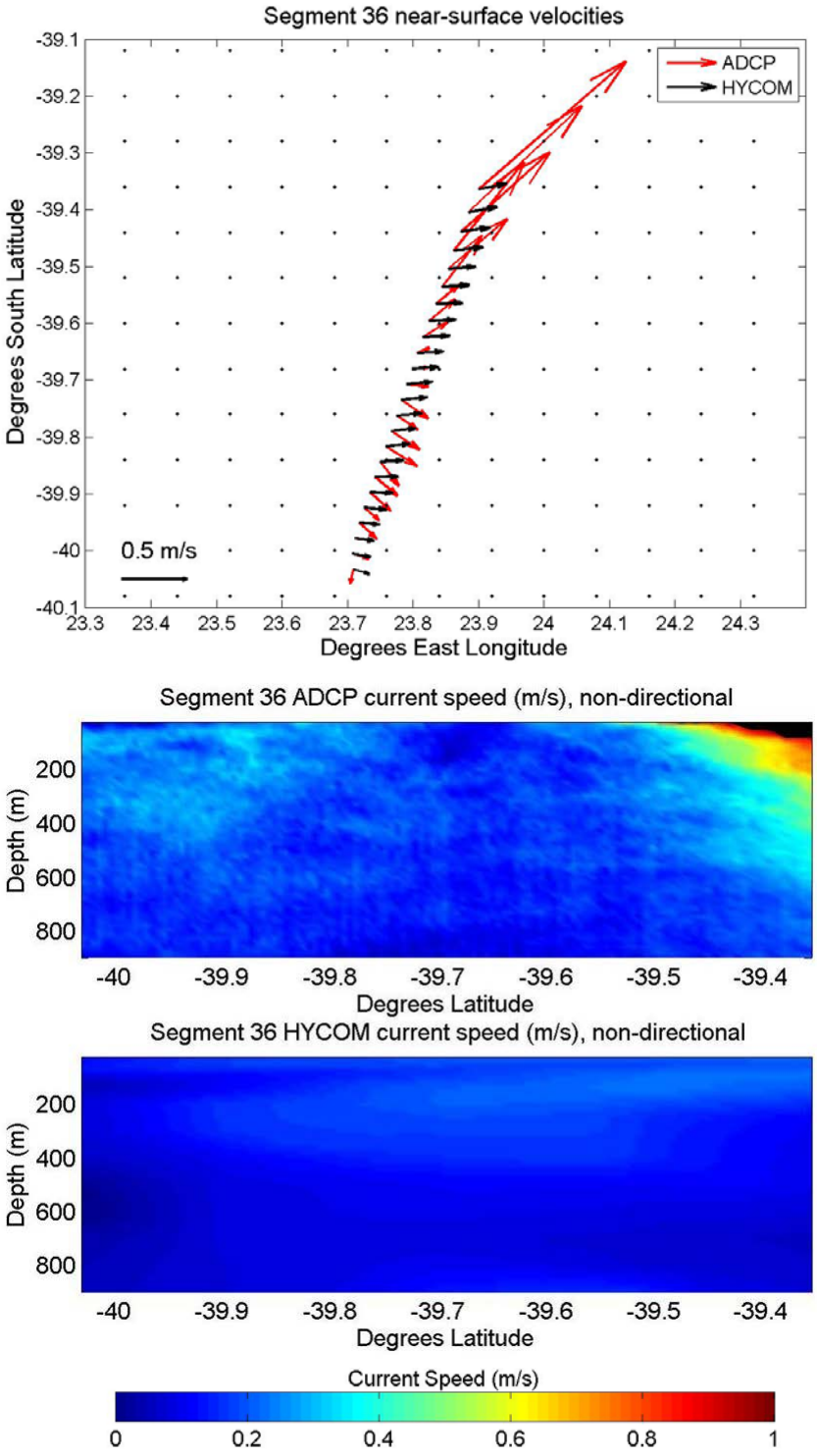

Figure 18. Segment 36 HYCOM and ADCP velocities. Near-surface velocities shown on top, ADCP velocity cross section in middle, and HYCOM velocity cross section at bottom. Velocities greater than 1 m/s are shown in black.

b. Segment 48, 5 February

Segment 48 included 68 data points along a 41.5 nm stretch of ocean, with a maximum observed velocity of 1.06 m/s and an average observed velocity of 0.12 m/s. Vectors shown in Figure 19 are thinned to every 3rd data point. Full HYCOM velocity fields for 5 February (Figure 38) show that the model placed the ARC 0.2˚ west of segment 48. HYCOM also placed the extreme western edge of a warm core eddy within segment 48. It is possible that HYCOM's depiction of southward flow along the lower half of segment 48 was a result of HYCOM either placing the eddy too far west or smoothing the transition in flow direction along the eddy's western edge.

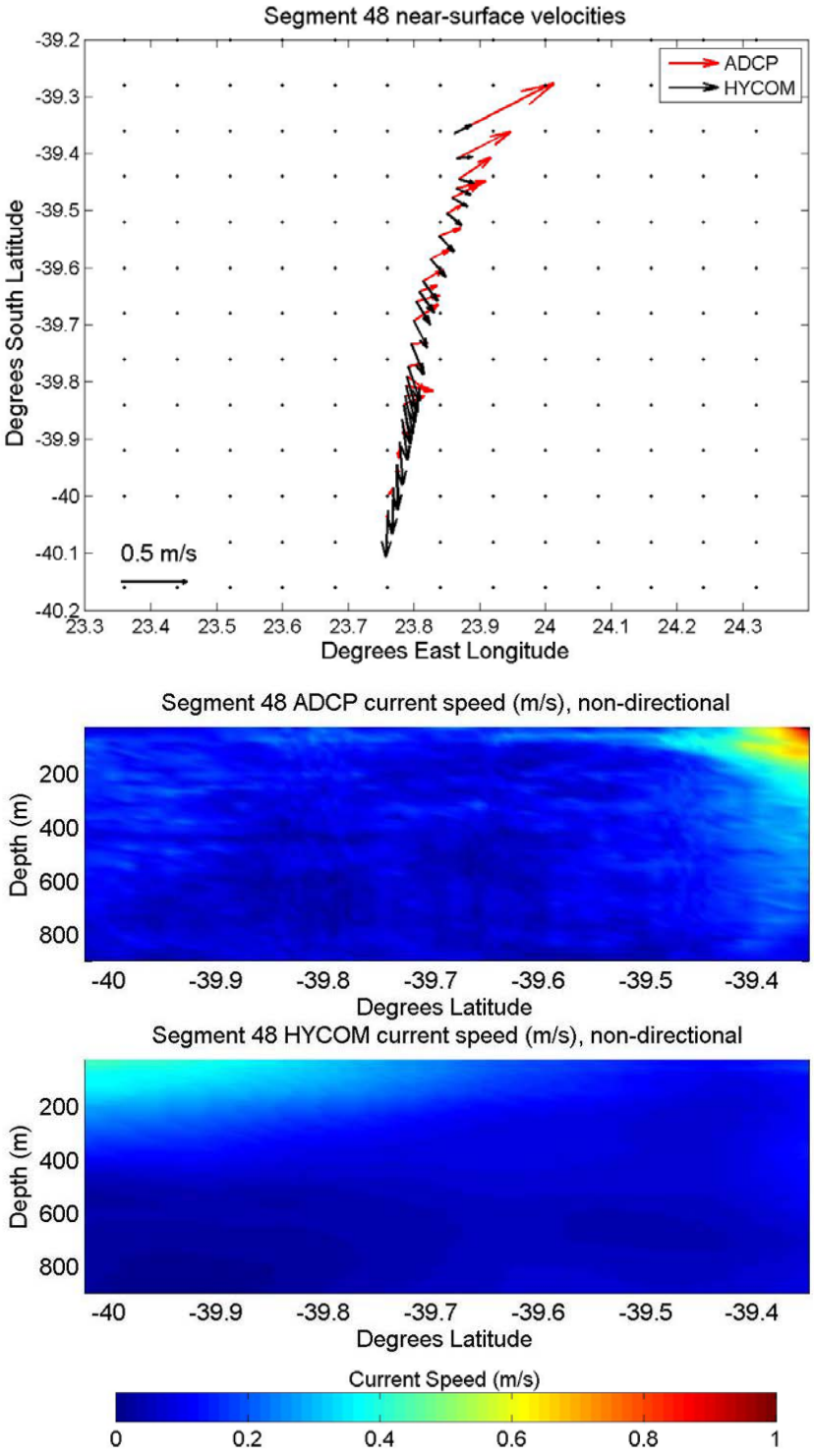

Figure 19. Segment 48 HYCOM and ADCP velocities. Near-surface velocities shown on top, ADCP velocity cross section in middle, and HYCOM velocity cross section at bottom. Velocities greater than 1 m/s shown in black.

C. ADDITIONAL COMPARISONS

Several non-repeated segments made for very interesting comparisons of the observed and modeled velocities. Segments 9 and 25 were examples of poor comparisons, segment 20 was an example of a fair comparison, and segments 3 and 51 were examples of good comparisons.

1. Segment 3, 25 January

Completed very early in the cruise, segment 3 consisted of a 45.2 nm northwest to southeast track, containing 140 data points, which began in the northwestern edge of the ARC. The maximum velocity observed in this segment was 1.62 m/s and the average velocity was 0.41 m/s. The near-surface velocity vectors in Figure 20 are thinned by a factor of 4, and show generally good agreement between HYCOM and the ADCP. The cross-sectional plot also show good placement of the current by HYCOM. Small spatial scale variations were, of course, smoothed over. HYCOM did not capture the full strength in the core of the current, nor the depth of the flow. The ADCP data shows a well-defined current to around 600 m depth, while the model only to 200 m depth.

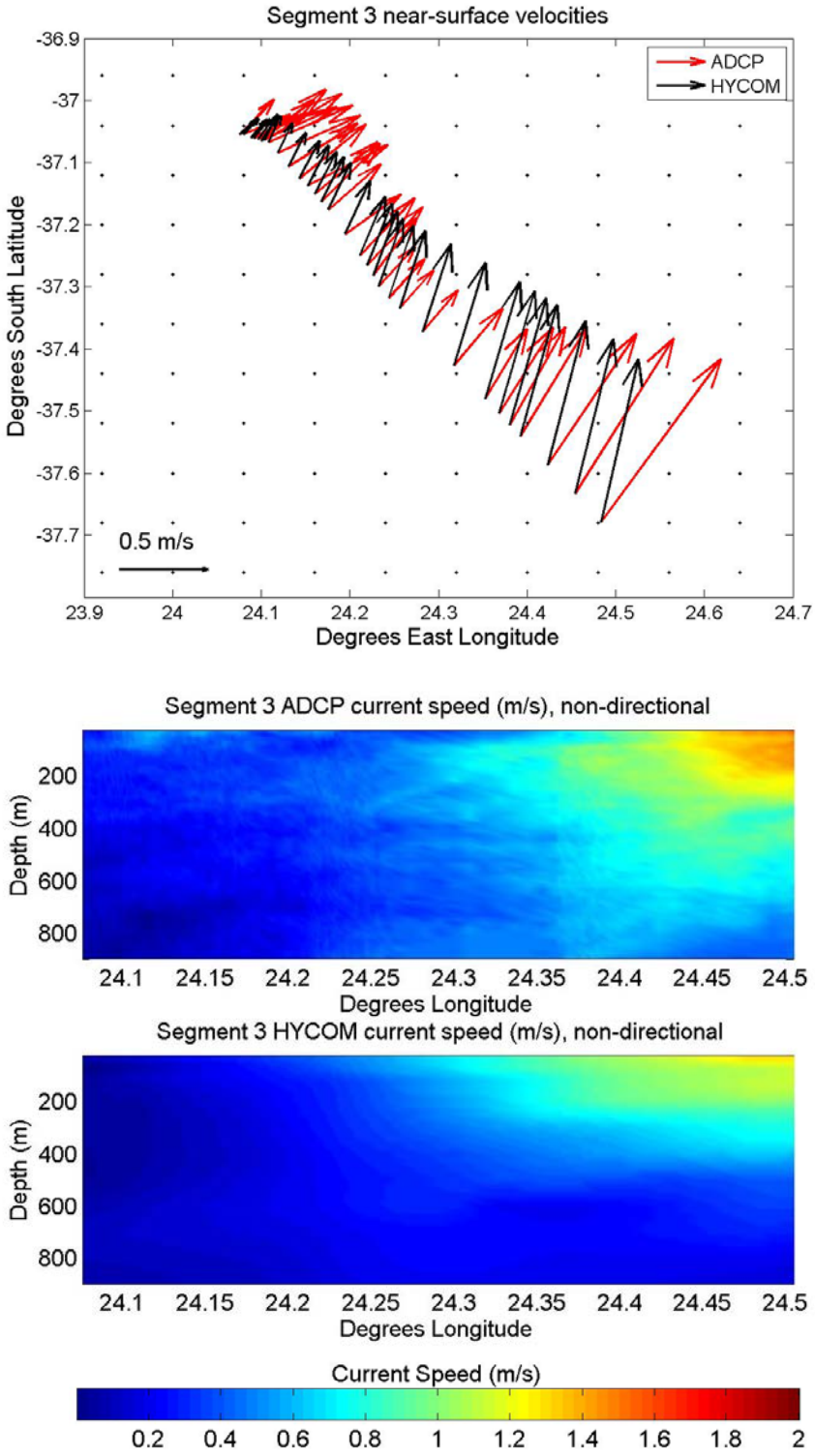

Figure 20. Segment 3 HYCOM and ADCP velocities. Near-surface velocities shown on top, ADCP velocity cross section in middle, and HYCOM velocity cross section at bottom.

2. Segment 9, 26 January

This segment included 72 ADCP data points along a 55.1 nm meandering southward track. An average velocity of 0.32 m/s was observed, with a maximum observed velocity of 0.74 m/s. One will immediately notice when viewing Figure 21 that modeled near-surface velocities were almost 90° different from the observed velocities (velocity vectors are thinned to every 4th vector). One should also note the maximum velocities in this transect were observed near the northern end of the track in the westward-flowing current, while HYCOM showed the bulk of the energy flowing southeastward along the southern end of the track. Segment 9's track passed through the middle of a complex interaction between the ARC and a warm core eddy, which obviously created a challenge for HYCOM simulations.

3. Segment 20, 28 and 29 January

Segment 20 was not directly compared to segments 19, 24, 33, and 37 due to its minimal temporal separation from segment 19, but includes features worth noting. A 64.4 nm west to east track with 219 data points, segment 20's average and maximum observed velocities were 0.27 and 0.85 m/s, respectively. In Figure 22, both the vector plot, which is thinned to every 5th data point, and the cross-sectional plot show how close the north-northeastward ARC is to the west-southwestward current in the eddy. Given the very close spacing between these features, HYCOM's performance was more impressive than the RMSE numbers in Table 3 indicate. HYCOM captured the eddy flow reasonably well, but performed a bit more poorly in capturing the direction of flow in the ARC.

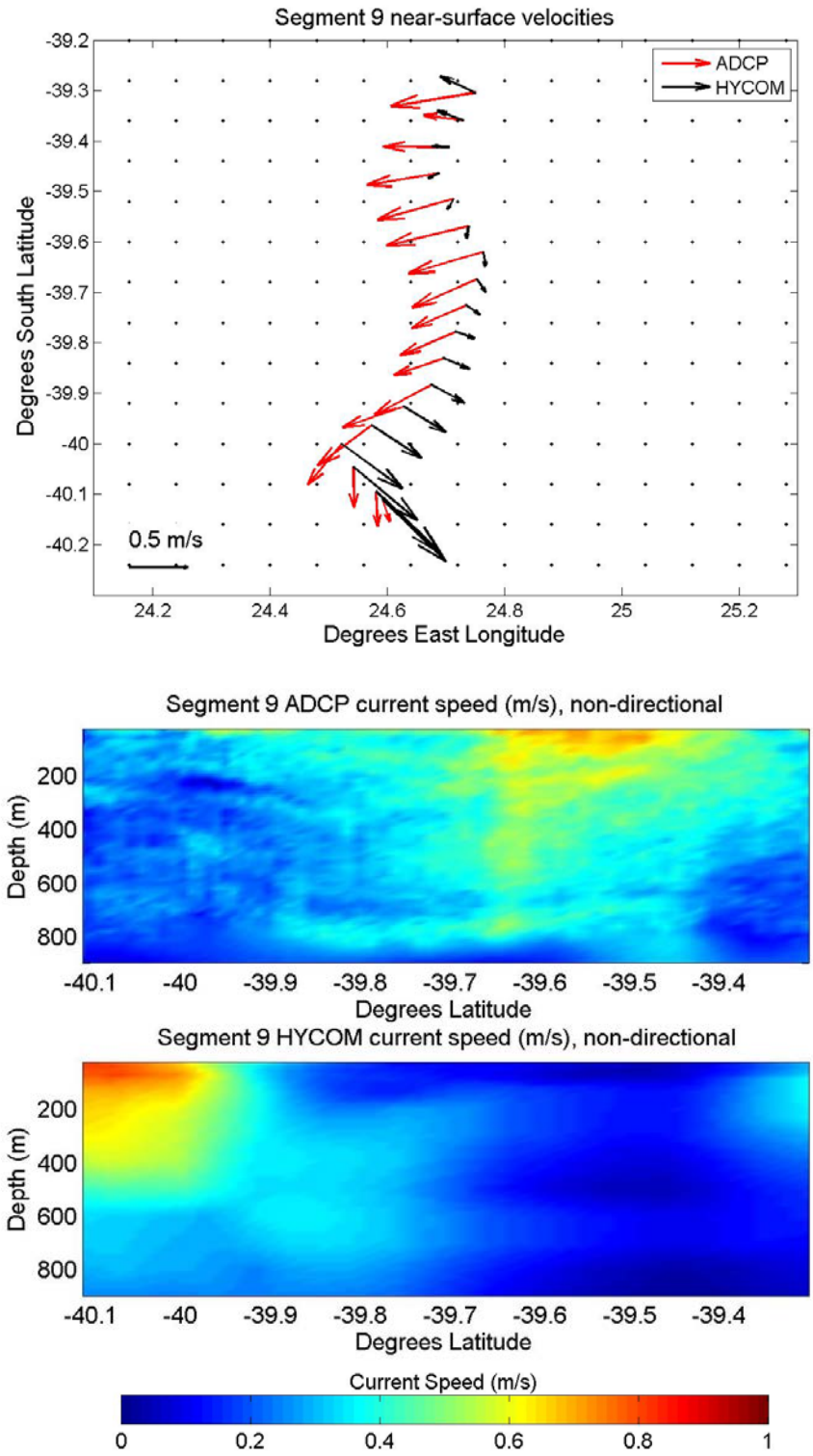

Figure 21. Segment 9 HYCOM and ADCP velocities. Near-surface velocities shown on top, ADCP velocity cross section in middle, and HYCOM velocity cross section at bottom.

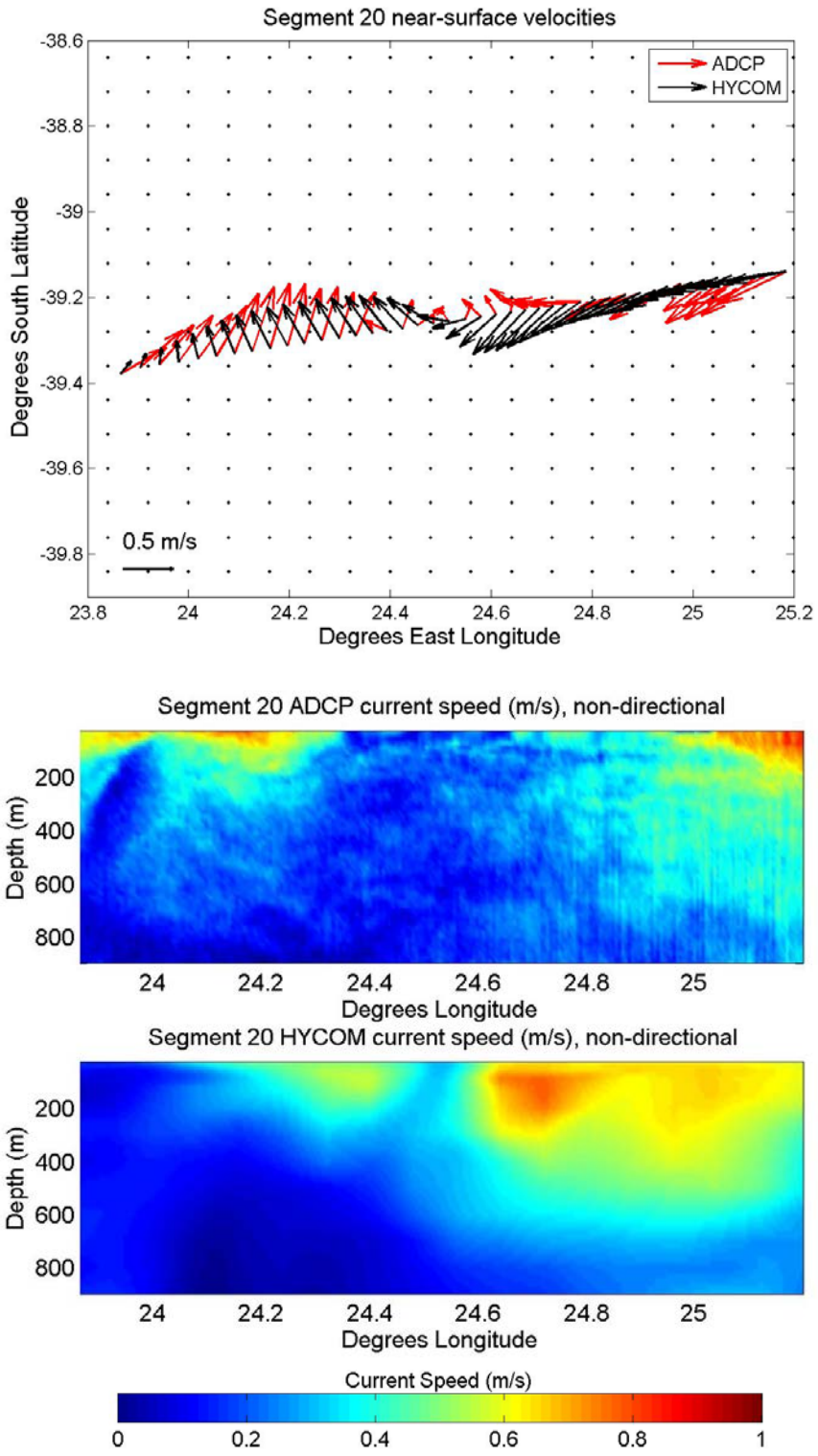

Figure 22. Segment 20 HYCOM and ADCP velocities. Near-surface velocities shown on top, ADCP velocity cross section in middle, and HYCOM velocity cross section at bottom.

4. Segment 25, 31 January

Only 18.3 nm long and consisting of 46 ADCP data points, segment 25 (with every 3rd velocity vector shown in Figure 23) was entirely in the ARC. This was one of the most energetic segments sampled, with a maximum observed velocity of 1.98 m/s and average velocity of 0.57 m/s. HYCOM clearly under-predicted the strength of the ARC at this location and did not accurately portray the direction. Given that this segment was only 18.3 nm long, crossing approximately 4 model grid points, a comparison based solely on the data collected here would be entirely unfair. However, given the highly positive portrayal of HYCOM in other segments chosen for comparison, it was important to display this less-than-ideal comparison. Either a temporal or spatial shift in HYCOM's depiction of the ARC may have caused the difference. The broader HYCOM velocity field in Figure 33 depicts stronger and more eastward flowing currents to the south of segment 25, indicating the possibility of a spatial error in the Agulhas Return Current's placement. Additionally, Figures 34-36 show that HYCOM increased the intensity of the ARC at segment 25's location in the days following 31 January. It is also possible, therefore, that the increase in intensity shown in Figures 34-36 began earlier than HYCOM depicted, but NCODA had not yet assimilated sufficient data to force the change.

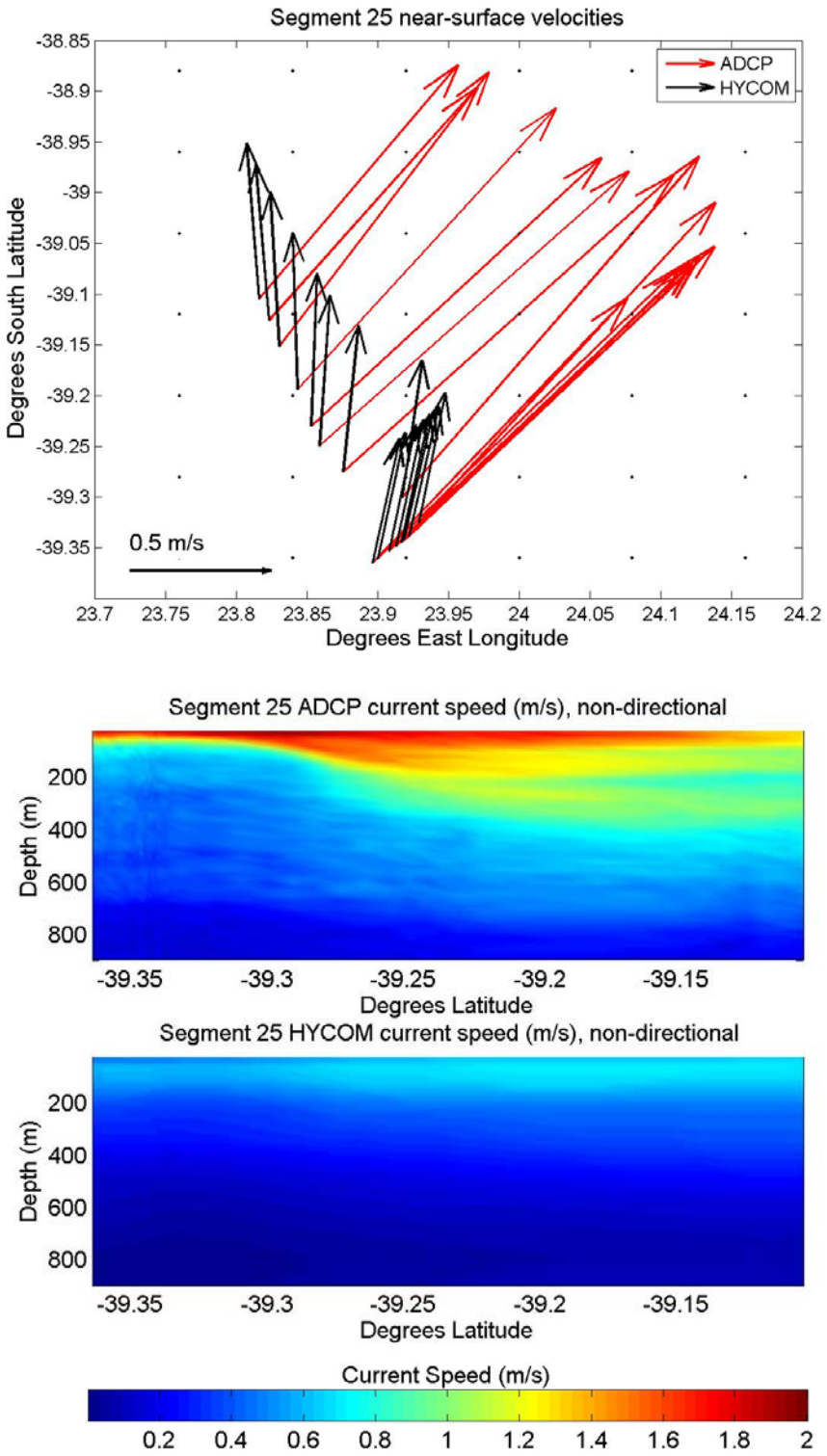

Figure 23. Segment 25 HYCOM and ADCP velocities. Near-surface velocities shown on top, ADCP velocity cross section in middle, and HYCOM velocity cross section at bottom.

5. Segment 51, 6 February

Segment 51 consisted of 63 data points along a 36.6 nm northwestward transect of the ARC. The average velocity recorded in this segment was 0.65 m/s, with a maximum observed velocity of 1.82 m/s. Although the vector plot in Figure 24 (every 4th point shown) shows large directional differences, the cross-sections compare favorably. HYCOM depicted a greater westward extent of the current core with less energy from 400 to 600 m in depth, but was fairly accurate in its depiction of the ARC's position and shape.

The differences observed between ADCP observations and HYCOM's modeling of this segment were very similar to those for segment 3 (Figure 20), except that HYCOM depicted a more accurate direction in segment 3. For both segments, HYCOM showed a northward bias and was missing some energy from 400 to 600 m depth, but generally captured the strength, shape, and location of the ARC. HYCOM best captured the ARC's direction in segment 33 (Figure 9), although, as with segment 51, HYCOM placed the bulk of the energy west of its ADCP observed location. Unlike with segments 3, 33 and 51, (where minor placement errors were observed) for segment 25 (Figure 23) HYCOM did not depict the strength of the ARC very accurately. This inaccuracy may have been due to a larger error in HYCOM's placement of the current. Given HYCOM's good depiction of segment 3 on 25 January, it is possible that 1) the model made errors in placement of the ARC that resulted in the poor depiction of segment 25 on 31 January, and 2) those errors were significantly smaller on the 1 February initialization due to subsequently assimilated altimetry.

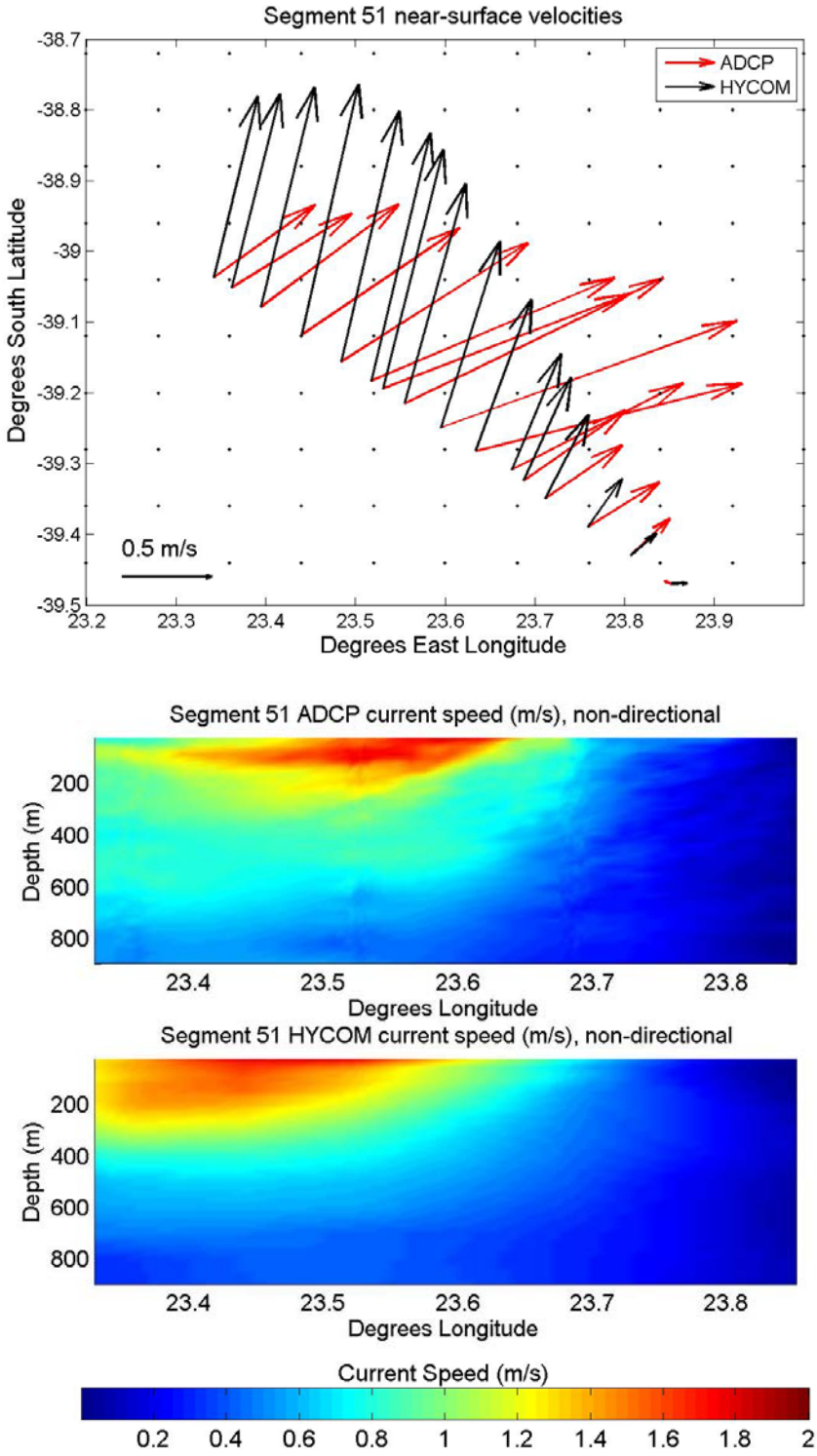

Figure 24. Segment 51 HYCOM and ADCP velocities. Near-surface velocities shown on top, ADCP velocity cross section in middle, and HYCOM velocity cross section at bottom.

V. DISCUSSION

This section will first discuss some precautions that should be noted when comparing densely sampled data with a model and when using RMSE for model-data comparisons. Next, the abrupt jump discontinuity noticed in the model between the 31 January and 1 February initializations will be discussed. Finally, some general statements will be made about HYCOM's performance in high- and low-energy regions.

A. OVERALL COMPARISON PRECAUTIONS

As previously stated, the track followed in ARC12 was chosen to sample a highly energetic ocean environment for testing seismic oceanography methods and studying mixing by mesoscale eddy stirring processes. It is not expected that any global model can perfectly capture the dynamic features observed during the cruise with today's level of technology. It is also important to note that many of the differences observed were a result of the very high resolution of ADCP sampling, which captured features that cannot be modeled at HYCOM's resolution. HYCOM was therefore challenged in this comparison to high resolution observations of the highly energetic features present along the ARC12 cruise track.

Metzger et al. (2008) included an RMSE velocity comparison between HYCOM and data obtained from two gliders crossing the Atlantic Ocean. The RMSE for those comparisons (along a path with less temporal variability than the ARC12 track) were 0.288 m/s and 0.298 m/s. The RMSE values for all ARC12 tracks were 0.35 m/s near-

surface, 0.26 m/s at 100-m, and 0.17 m/s at 500-m, consistent with the comparison to glider data. Especially considering the high variability and energy present in the ARC12 region, these numbers are very promising.

One should understand that RMSE statistics are skewed unfavorably against HYCOM. Given the spatial velocity gradients observed throughout ARC12, a shift in current location of only a few tenths of a degree could result in a major jump in RMSE. Studying the mismatch in stream coordinates by spatially shifting the model fields to align with observed features could be a topic for further research.

One should be cautioned that the method of weighted RMSE calculation used in this comparison can create significantly higher error statistics for low speed flow when dividing even minor speed differences by a very small observed speed. One should also note that the method of calculation used for direction RMSE gives the same weight to direction errors for near zero velocities (when current direction determinations become inaccurate or ill-defined) as it does for high velocities.

To determine if oversampling of the model led to inaccurate error statistics, RMSE was recalculated using only data points greater than 0.2 nm from any other point, which (because data were averaged at 5 minute intervals) removed all data for periods when the ship speed was less than 2.4 knots. These new RMSE values, shown at the top of Table 5, differed very little from RMSE shown in Table 3. Therefore, oversampling was not a significant factor in the error statistics.

An additional layer of filtering was subsequently applied to remove, from comparison, areas where the ADCP-recorded near-surface currents were below a certain value. As Table 5 shows, when minimum speed for comparison was increased, raw speed RMSE increased, while both raw direction RMSE and weighted speed RMSE decreased. As discussed, the decrease in direction and weighted speed RMSE are to be expected, given the biases inherent in the techniques used to calculate those statistics.

Min	Data	Weighted speed RMSE			Speed RMSE (m/s)			Direction RMSE (degrees)		
Speed (m/s)	Points	Surface	100-m	500-m	Surface	100-m	500-m	Surface	100-m	500-m
0.00	2521	101.0%	60.0%	48.0%	0.36	0.26	0.18	44.38	37.38	31.23
0.25	2064	50.0%	52.0%	41.0%	0.38	0.27	0.19	34.87	32.25	28.45
0.50	1351	42.0%	39.0%	39.0%	0.44	0.30	0.21	26.91	24.03	25.43
0.75	851	40.0%	32.0%	37.0%	0.54	0.34	0.24	22.23	20.71	20.76

Table 5. Filtered RMSE.

B. JUMP DISCONTINUITY IN MODEL INITIALIZATION

Figure 5 clearly shows an abrupt change between model initializations. Figure 6 shows that there were significant changes observed during the period from 28 January to 01 February. However, the speed increase observed by the shipboard ADCP was only 0.30 m/s per day from 28 to 30 January and 0.26 m/s per day from 30 January to 1 February, whereas HYCOM increased forecast speed by 0.98 m/s in only 24-hours between initializations on 31 January and 01 February. This indicates that HYCOM assimilated significantly different data during the HYCOM-NCODA runstream leading up to the 01 February initialization than it assimilated 24-hours prior.

Understanding the timeliness and effectiveness of the initialization and assimilation process should be a future research project.

HYCOM-modeled velocities in segment 33, (Figure 9) where this significant shift occurred, compared very favorably to ADCP-observed velocities, particularly when low-energy regions outside the current core were not considered. A comparison of Figure 9's temporally and spatially interpolated HYCOM values from 3-hourly model output versus Figure 5's purely spatial interpolation of 24-hourly model fields shows that temporal variability and assimilation updates can significantly affect the modeled conditions. Anyone using HYCOM to make characterizations of the ocean environment in a temporally variable region should be aware that no one model tau can be considered representative of conditions for an entire day. It is therefore very important to match the closest model tau to the forecast valid time, and analyze any temporal changes that may occur during the forecast period.

C. MAJOR, PERSISTENT FEATURES

HYCOM accurately simulated placement of the major features observed during ARC12, including the Agulhas Current, ARC, and the warm core eddy east of the ARC. Exact placement of features was sometimes off by several tenths of a degree, as determined by a comparison between individual segment plots and broader-scale HYCOM output in Appendix A. Even when a feature was somewhat misplaced, its general shape was usually accurately defined. Significant spatial variability existed at the sub-grid scale level, so HYCOM was not able to properly portray the

exact shape of some features. When considering the RMSE numbers, especially those for velocity, one must recognize that minor misplacement of features penalized the model heavily.

D. WEAK AND INCONSISTENT FEATURES

HYCOM was qualitatively less accurate in regions of small-scale variations that were observed during ARC12. In many instances, regions just outside of a jet of current were characterized by sub-grid scale turbulent flow, which HYCOM was unable to properly depict. HYCOM had noticeable discrepancies from observations in the region where there was interaction between the ARC and a warm core eddy. Although the more energetic features in this area were reasonably well depicted, many of the weaker flows in this interaction region were poorly depicted. Table 5 would suggest that overall HYCOM performed more poorly in regions of weaker flow than stronger flow. This is not necessarily true, as the methods of RMSE calculation used in this comparison can overinflate error statistics for low speed flows.

THIS PAGE INTENTIONALLY LEFT BLANK

VI. CONCLUSIONS AND SUGGESTIONS FOR FUTURE RESEARCH

A. CONCLUSIONS

Velocity fields produced by HYCOM, the Navy's latest operational ocean forecast model, were systematically evaluated through comparison with actual ADCP velocities collected during a two-week ARC12 cruise. These ADCP data allowed for a rare opportunity to make model-data comparisons of velocity fields, whereas most model-data comparisons use temperature in their comparisons. Both quantitative and qualitative comparisons were made, which lead to a better understanding of HYCOM and its uncertainties as an operational model.

Understanding of HYCOM's performance is crucial as this model will be used to make ocean predictions that directly affect naval operations across multiple warfare disciplines, but primarily in undersea warfare (USW). Knowledge of both the ocean environment and uncertainty in oceanography's portrayal of that environment are crucial to successful USW operations.

A naval oceanographer must fully understand the tools at his or her disposal in order to accurately characterize the battlespace. With every forecasting or analysis tool comes a degree of uncertainty. HYCOM is obviously not perfect, but, considering the challenging environment for which this comparison was conducted, the model performed remarkably well.

One should be aware of the limitations of the HYCOM model. For USW applications, knowing the exact placement of a front can yield a tremendous advantage. As observed

during multiple transects into the southern side of the Agulhas Return Current, HYCOM misplaced the front by up to 0.6˚, which is substantial. However, the fact that the front exists in the vicinity is still very useful information, if the appropriate degree of uncertainty about its exact location can be properly communicated.

HYCOM demonstrated an ability to capture the most energetic and persistent features with reasonable accuracy. Core current speed was generally underforecast, but placement of the current core was normally very good.

B. FUTURE RESEARCH

1. Sensitivity to Spatial Shifts

Using the same data sets analyzed in this thesis, one could incorporate multiple spatial shifts in either data set to see how error statistics could change.

2. Analysis Using Additional ARC12 Data

Additional data collected during ARC12 include 203 expendable bathythermeographs and 57 CTD casts, which included 39 casts by an underway CTD. Further analysis using these data could reveal more detailed information about HYCOM’s performance.

3. Effect of Velocity Errors on Sound Speed Profile

From a USW perspective, it would be important to understand how the observed velocity errors relate to sound speed profile errors.

4. Assimilation Scheme

Given the 0.98 m/s difference in current speed between analyses, it may be useful to conduct an evaluation of HYCOM’s assimilation scheme.

5. Transition to NAVGEM

AS HYCOM transitions atmospheric forcing from NOGAPS to NAVGEM, there is opportunity to study the impact this change will have on HYCOM’s effectiveness.

THIS PAGE INTENTIONALLY LEFT BLANK

APPENDIX. HYCOM SURFACE CURRENTS

Figures 25 through 40 show HYCOM analyzed surface velocities valid 00Z for the 23 January to 07 February 2012. The ARC12 cruise track is shown in black. A red highlight along the track indicates the portion of the track covered during the same day as the associated HYCOM model run.

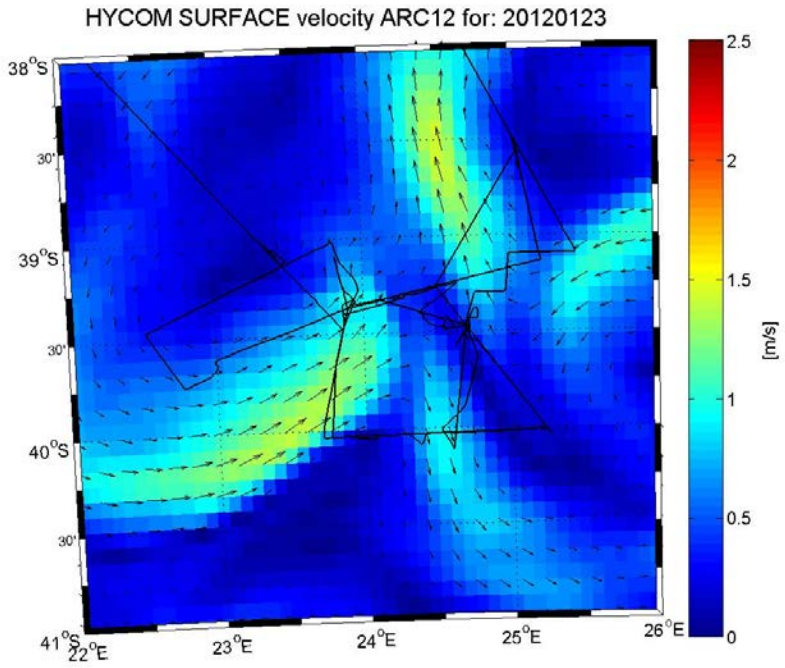

Figure 25. HYCOM surface velocities for 23 January 2012.

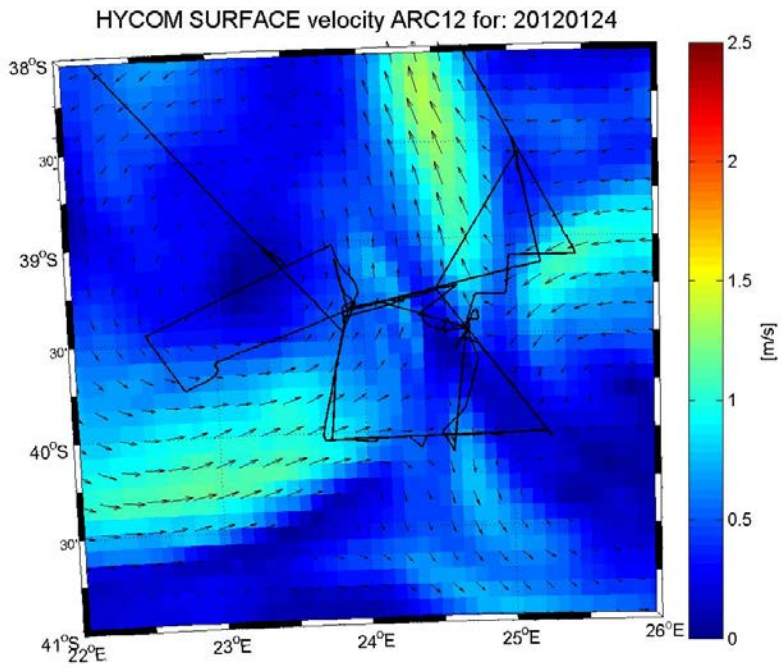

Figure 26. HYCOM surface velocities for 24 January 2012.

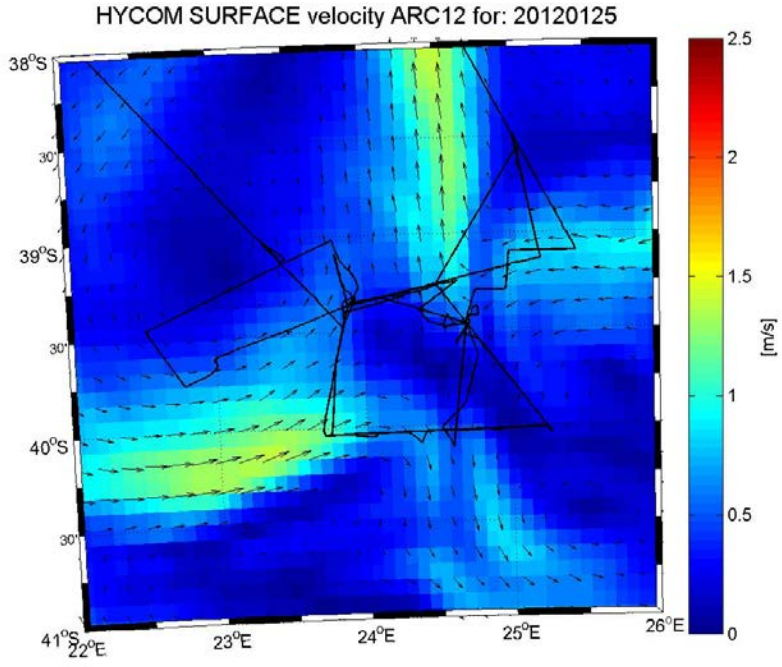

Figure 27. HYCOM surface velocities for 25 January 2012.

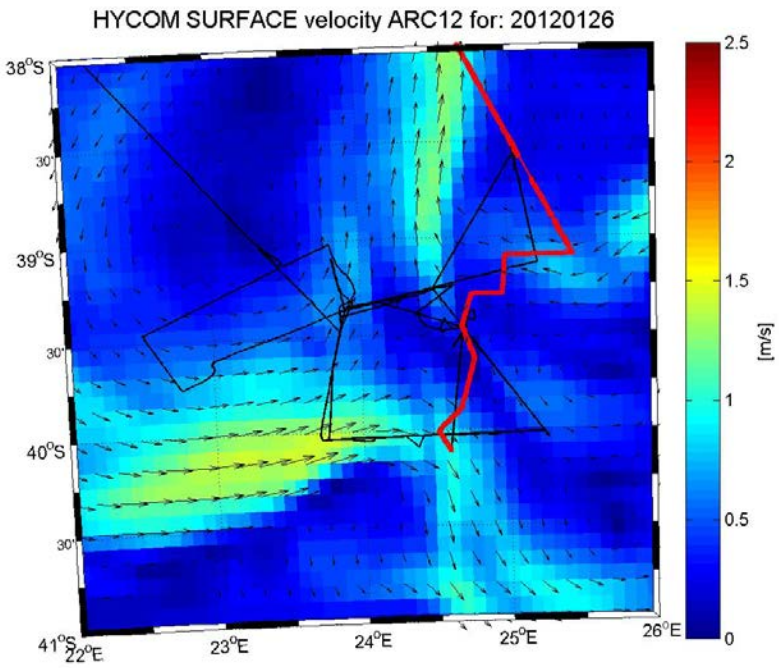

Figure 28. HYCOM surface velocities for 26 January 2012.

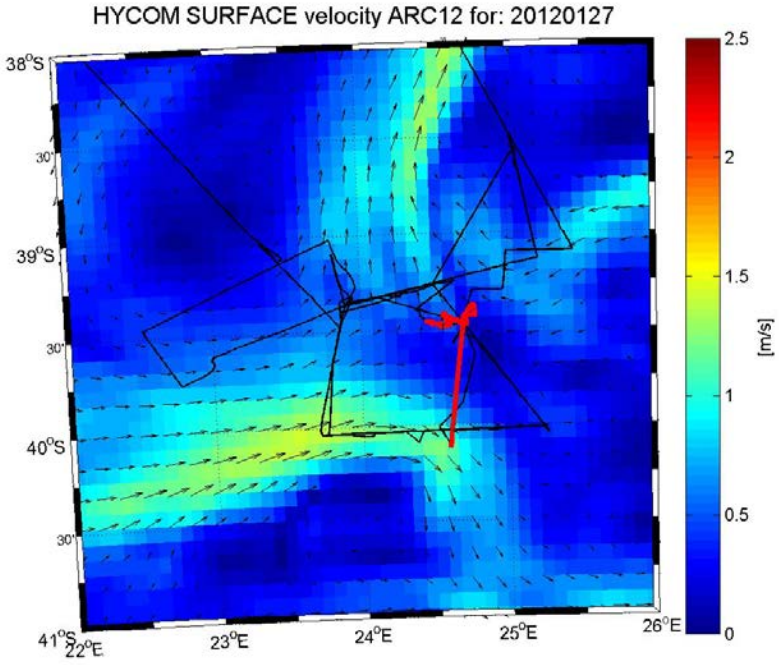

Figure 29. HYCOM surface velocities for 27 January 2012.

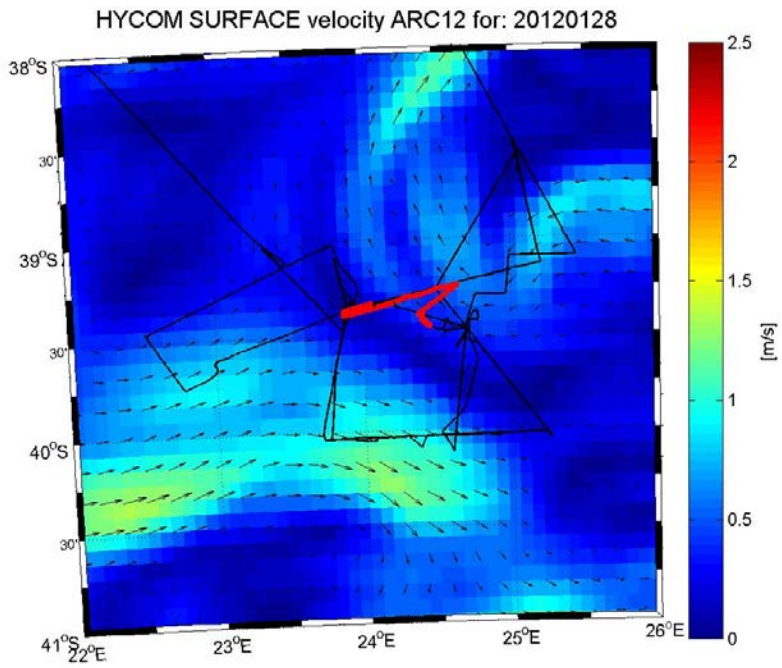

Figure 30. HYCOM surface velocities for 28 January 2012.

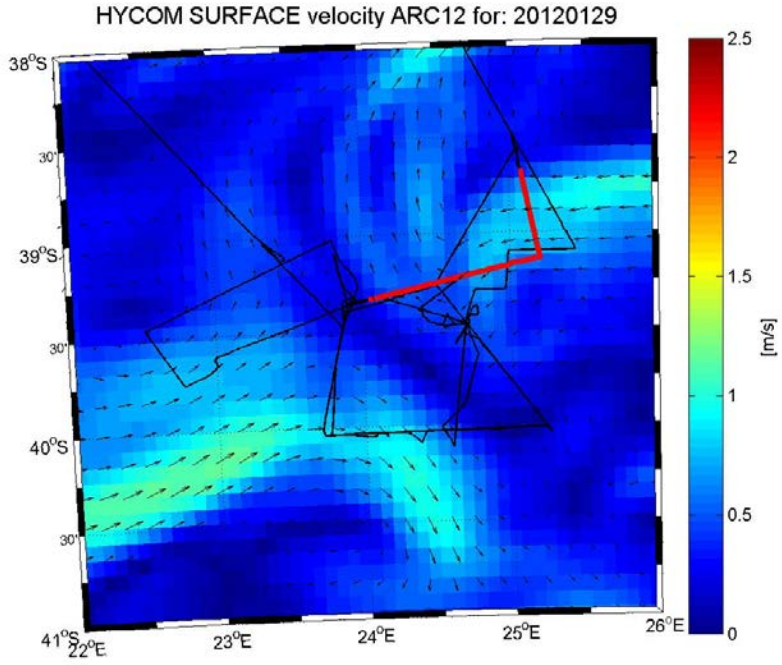

Figure 31. HYCOM surface velocities for 29 January 2012.

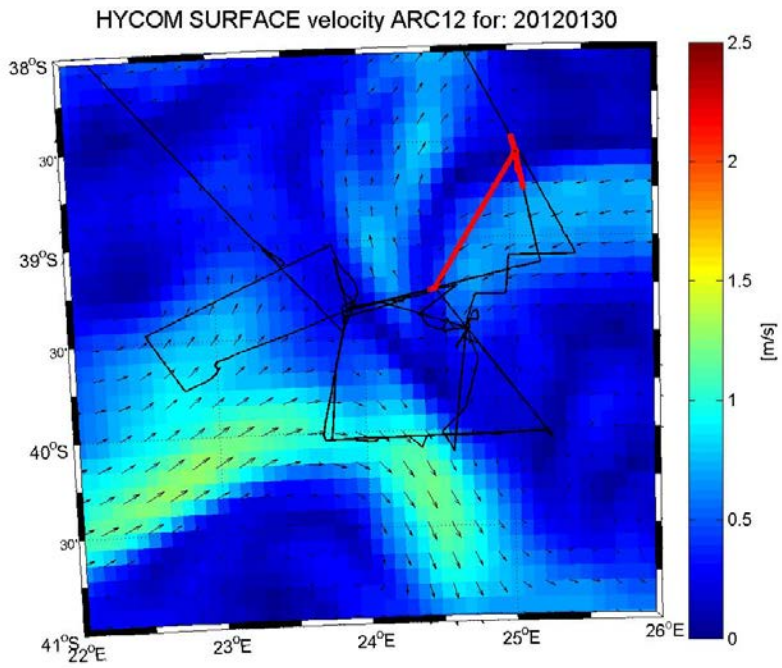

Figure 32. HYCOM surface velocities for 30 January 2012.

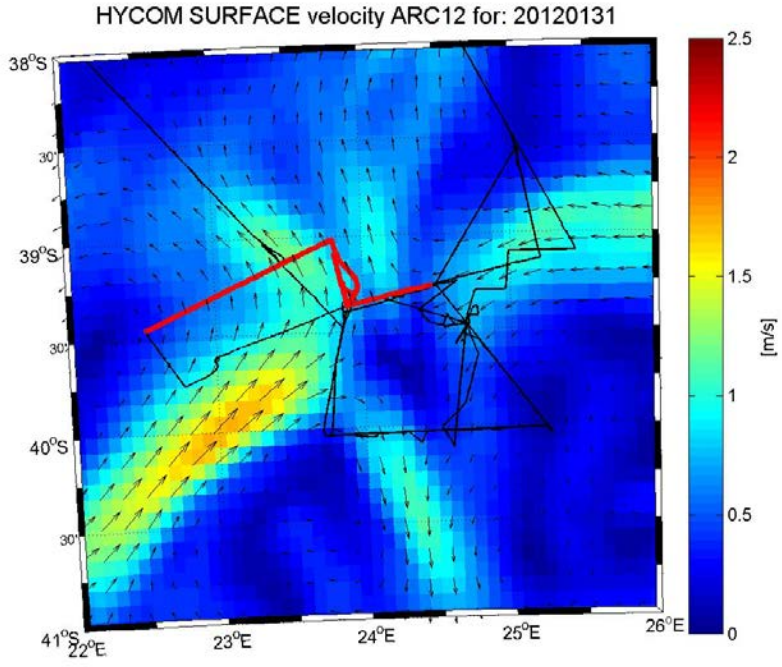

Figure 33. HYCOM surface velocities for 31 January 2012.

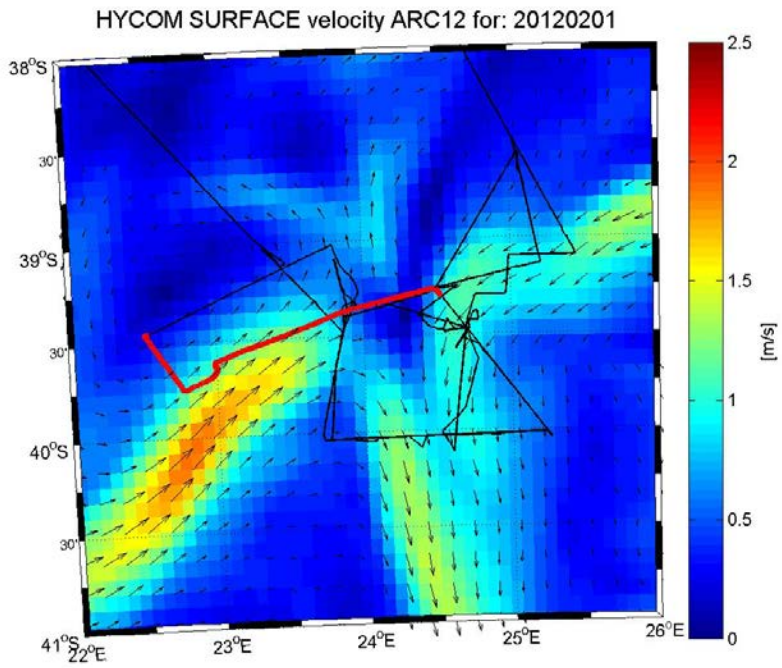

Figure 34. HYCOM surface velocities for 01 February 2012.

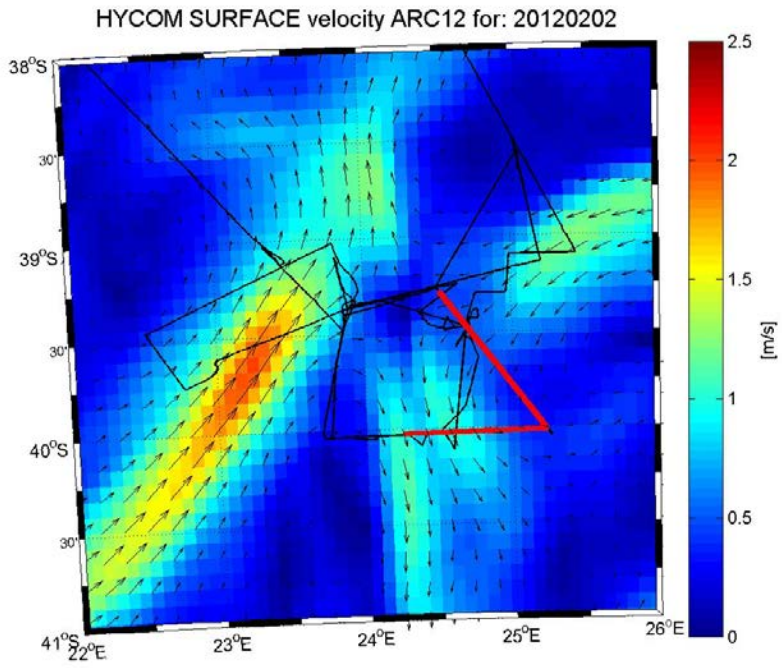

Figure 35. HYCOM surface velocities for 02 February 2012 (24-hr forecast from 01 February analysis).

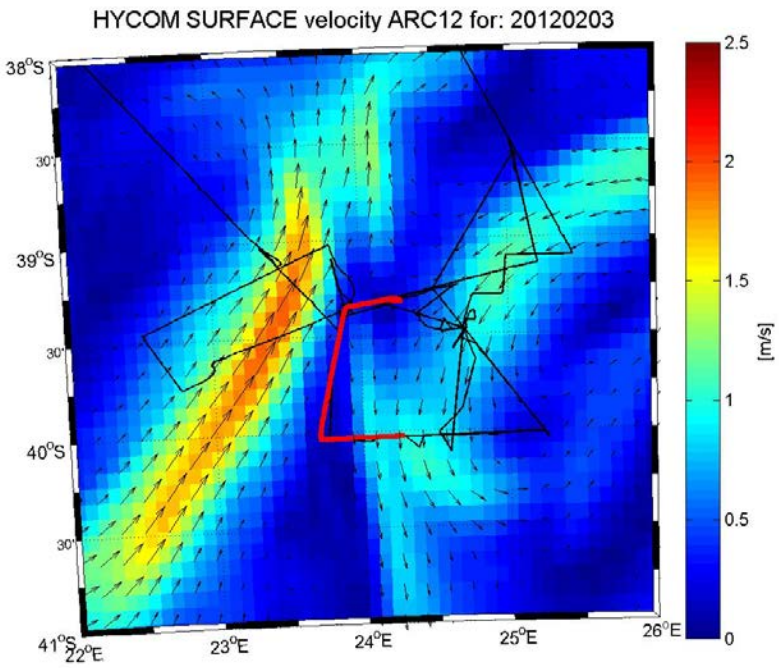

Figure 36. HYCOM surface velocities for 03 February 2012.

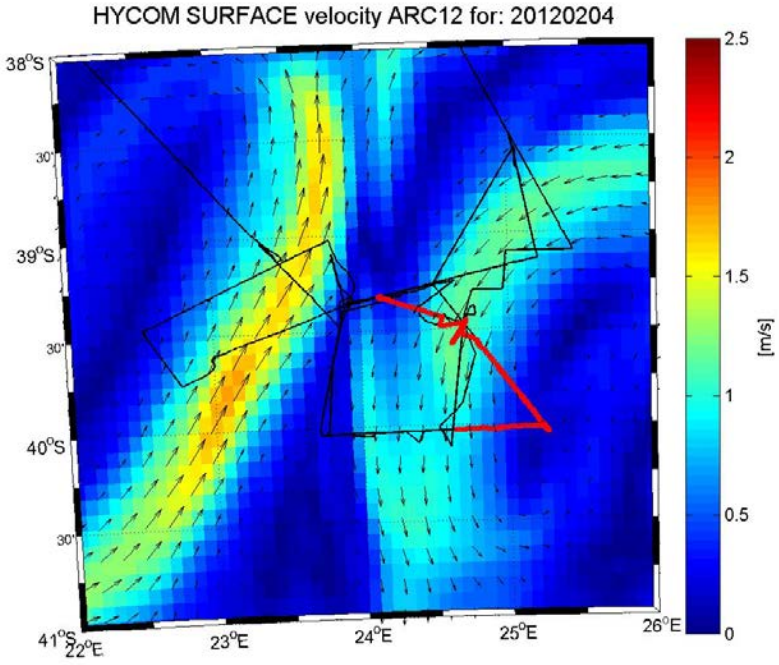

Figure 37. HYCOM surface velocities for 04 February 2012 (24-hr forecast from 03 February analysis).

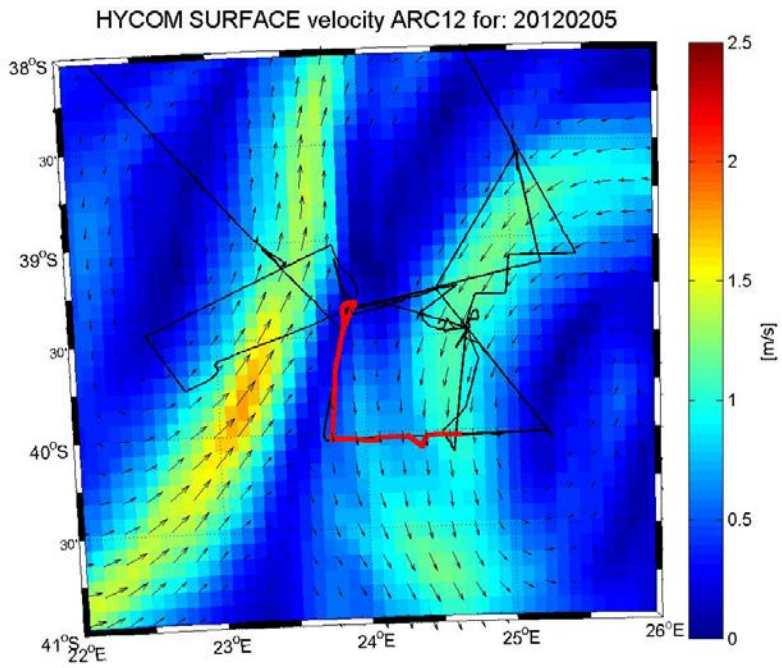

Figure 38. HYCOM surface velocities for 05 February 2012.

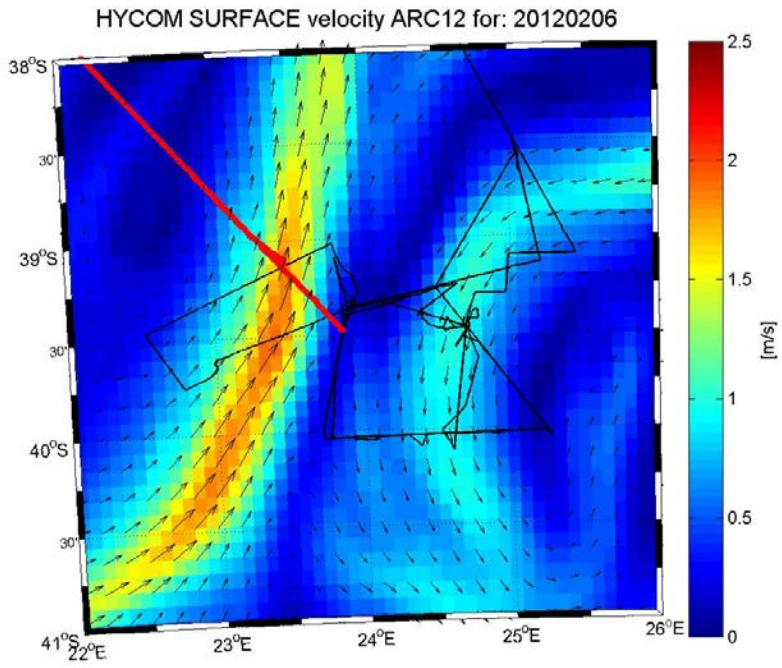

Figure 39. HYCOM surface velocities for 06 February 2012.

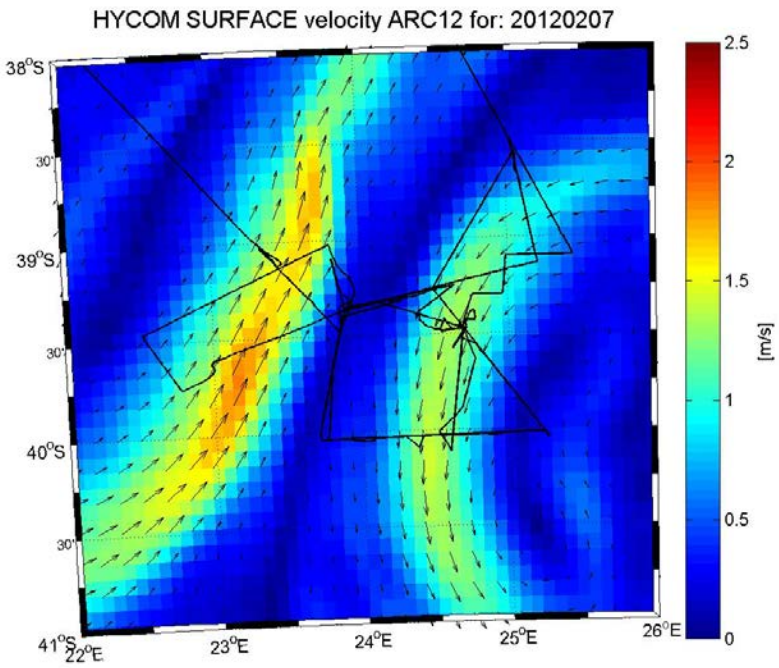

Figure 40. HYCOM surface velocities for 07 February 2012.

THIS PAGE INTENTIONALLY LEFT BLANK

LIST OF REFERENCES

Barron, C. N., A. B. Kara, P. J. Martin, R. C. Rhodes, and L. F. Smedstad, 2006: Formulation, implementation and examination of vertical coordinate choices in the global Navy Coastal Ocean Model (NCOM). *Ocean. Model.,* **11,** 347-375, doi:10.1016/j.ocemod.2005.01.004.

Beal, L. M., and H. L. Bryden, 1999: The velocity and vorticity structure of the Agulhas Current at 32˚S. *J. Geophys. Res.,* **104,** 5151–5176.

Bleck, R., C. Rooth, D. Hu, and L. Smith, 1992: Salinity-driven thermocline transients in a wind- and thermohaline-forced isopycnic coordinate model of the North Atlantic. *J. Phys. Oceanogr.*, **22**, 1486-1505.

Bleck, R., 2002: An oceanic general circulation model framed in hybrid isopycnic-Cartesian coordinates. *Ocean. Model.,* **37,** 55-88.

Book, J. W., A. E. Rice, W. T. Wood, C. Barron, I. Ansorge, and R. Roman, 2012: Warm-core Agulhas Plateau Eddies. *AGU Chapman Conference, The Agulhas System and its Role in Changing Ocean Circulation, Climate, and Marine Ecosystems,* Stellenbosch, South Africa, 8-12 October, 2012. (Available at: http://chapman.agu.org/agulhas/files/2012/11/Book.pdf)

Cummings, J. A., 2005: Operational multivariate ocean data assimilation. *Q. J. R. Meteorol Soc.,* **131,** 3583-3604, doi_10.1256/qj.05.105.

Fox, D. N., W. J. Teague, C. N. Barron, M. R. Carnes, and C. M. Lee, 2002: The Modular Ocean Data Assimilation System (MODAS). *J. Atmos. Ocean. Technol.,* **19,** 240-252.

Gordon, A. L., J. R. E. Lutjeharms, and M. L. Grundlingh, 1987: Stratification and circulation at the Agulhas Retroflection. *Deep Sea Res.,* **34,** 565–599.

Halliwell, G. R., 2004: Evaluation of vertical coordinate and vertical mixing algorithms in the HYbrid-Coordinate Ocean Model (HYCOM). *Ocean. Model.,* **7,** 285-322, doi:10.1016/j.ocemod.2003.10.002.

Jacobs, S. S., and D. T. Georgi, 1977: Observations on the Southwest Indian/Antarctic Ocean, Pp. 43–84 in A Voyage of Discovery. M. Angel, ed., Supplement to *Deep Sea Res.*, **24,** 43-84.

Lutjeharms, J. R. E., and H. R. Valentine, 1988: Eddies at the Sub-Tropical Convergence south of Africa. *J. Phys. Oceanogr.,* **18,** 761-774.

Lutjeharms, J. R. E., and I Ansorge, 2001: The Agulhas Return Current. *J. Mar. Syst.,* **30,** 115–138.

Lutjeharms, J. R. E., 2007: Three Decades of research on the greater Agulhas Current. *Ocean Sci.,* **3,** 129-147, doi:10.5194/os-3-129-2007.

Metzger, E. J., H. E. Hurlburt, A. J. Wallcraft, J. F. Shriver, L. F. Smedstad, O. M. Smedstad, P. Thoppil, D. S. Franklin, 2008: Validation Test Report for the Global Ocean Prediction System V3.0 – 1/12° HYCOM/NCODA: Phase I. NRL Memo. Report, NRL/MR/7320—08-9148. (Available at http://www7320.nrlssc.navy.mil/pubs.php), 82 pp.

Metzger, E. J., H. E. Hurlburt, A. J. Wallcraft, J. F. Shriver, Townsend, T. L., O. M. Smedstad, P. G. Thoppil, D. S. Franklin, 2010: Validation Test Report for the Global Ocean Prediction System V3.0 – 1/12° HYCOM/NCODA: Phase II. NRL Memo. Report, NRL/MR/7320—10-9236. (Available at http://www7320.nrlssc.navy.mil/pubs.php), 70 pp.

Stramma, L., 1992: The South Indian Ocean Current. *J. Phys. Oceanogr.,* **22,** 421-430.

Teague, W. J., M. J. Carron, and P. J. Hogan, 1990: A comparison between the Generalized Digital Environmental Model and Levitus climatologies. *J. Geophys. Res.,* **95** (C5), 7167-7183.

Thoppil, P. G., J. G. Richman, and P. J. Hogan, 2011: Energetics of a global ocean circulation model compared to observations. *Geophys. Res. Lett.,* **38,** L15607, doi:10.1029/2011GL048347.

INITIAL DISTRIBUTION LIST

1. Defense Technical Information Center
   Ft. Belvoir, Virginia

2. Dudley Knox Library
   Naval Postgraduate School
   Monterey, California